Politecnio di Torino
Corso di Laurea Magistrale in Ingegneria Elettrica
University of Nottingham

Tesi di Laurea Magistrale

High-performance control for electric drives

Relatori:
Prof. Radu Bojoi
Prof. Pericle Zanchetta
Dr.Shafiq Ahmed Odhano
Dr. Silvio Vaschetto

Candidato:
Valerio Vodola

Anno Accademico: 2018/2019

Ai miei genitori, a mia sorella e alla mia famiglia...

Abstract

The control of electric motors today is one of the most interesting topics in the field of electrical engineering. In the industrial sector, one of the most used electric motors is, without any doubt, the three-phase induction motor due to its numerous features, like the low costs of construction and its high robustness. For this reason, the study of control for induction motors is and will remain a topic of interest in the field of electrical drives.

So far, two of the most used control strategies are represented by the Field Oriented Control and the Direct Torque Control that allow us to satisfy most of the industrial applications. However, in recent years, thanks to the increase in the microcontroller computational power, new control strategies, such as the Model Predictive Control (MPC), have become promising alternatives in the field of high performance drives.

The most common implementation of a MPC-type strategy, the so-called FCS-MPC, aims at minimizing a single cost function by assigning a weighting factor to give more or less importance to the minimization of the torque or the flux error. However, the main disadvantages of the conventional FCS-MPC are related to the definition of the weighting factors, as well as to the variable switching frequency that strongly depends on the operating conditions.

In this thesis, in order to overcome these two issues, I have conducted a theoretical analysis followed by simulations and experimental tests of various control strategies. They go under the name of Sequential Model Predictive Control (SMPC) and they have the advantage of avoiding the use of weighting factors. These strategies were tested on a three-phase induction motor powered by a 2-Level Voltage Source Inverter.

The simulations that I have carried demonstrate the existence of six possible SMPC-type strategies that allow to control the IM. After a careful analysis of those various SMPC strategies, I have chosen the one that showed the lowest current and torque ripples and I have also implemented a modulator in order to fix the switching frequency. Furthermore, I have showed that the implementation of the modulator, in addition to make constant the switching frequency, resulted in excellent performances in terms of current and torque ripple.

Finally, I have conducted experimental tests that turned out to be in perfect agreement with the theoretical analysis and the simulations. The results obtained demonstrate that it is possible to control stator flux and torque separately without using weighting factors, obtaining excellent dynamic performances and at the same time, through the implementation of the modulator, very low harmonic distortion values.

Contents

Introduction

The control of electrical machines, is one of the most common challenges in the field of electrical engineering. In the industrial sector, among the most used electric motors, there is certainly the three phase induction motor (IM), which is also characterized by low construction costs and high robustness. From this point of view, the study of electric drives for IM is and will remain a topic of interest in the field of electrical drives.

At present, the Field Oriented Control (FOC) and the Direct Torque Control (DTC) are among the most used strategies in electric drives and with these strategies it is possible to satisfy most industrial applications. However, in recent years, thanks to the significantly higher microcontroller computational power, it has been possible to implement new control strategies including the Model Predictive Control (MPC), therefore at present, a possible alternative in the field of high performance drives is the MPC.

The MPC technique is widely used in many industrial sectors and not only in the field of electric drives [1–3]. The first ideas of MPC were developed in the 1960s as an application of the theory of optimal control. The first applications of the MPC in power electronics/electrical drives occurred at the beginning of 1980s, in high power systems with low switching frequency [4]. The main feature of the MPC is to use the model of the system, in order to predict the future behavior of the variables to be controlled. In particular, the variables are predicted up to a predefined time horizon in order to select the optimal actuations, according to the established optimization criterion. Among the main advantages of the MPC in the field of electric drives there is the possibility of obtaining high dynamic performance and the low tuning work necessary for their implementation.

Until now, the Finite Control Set-MPC (FCS-MPC) of torque and flux of AC machines has been implemented using a single cost function and using a weighting factor to give more or less importance to the minimization of torque or flux error [5, 6]. The calculation of the weighting factor is one of the main problems in this control strategy.

A possible solution for predictive torque and flux control for AC machine that does not use weighting factors is the Sequential Model Predictive Control (SMPC). Since these strategies realize the minimization of the cost functions associated to the error flux and error torque in two different control stages. In particular, at each control stage the number of usable voltage vectors is reduced, and finally the optimal voltage vector selected from the

second control stage is applaied through the inverter. It is interesting to observe how the possible SMPC strategies are different and can be distinguished by considering which cost function and in which control stage it is evaluated and how many voltage vectors are available for the minimization of the cost function in the second control stage.

In the first part of this thesis, all the possible SMPC strategies that use two control stages to control stator flux and torque separately are studied, identifying which of them allow to control the IM when a 2 Level-Voltage Supplay Inverter (2L-VSI) is used to power it.

Like the FCS-MPC of torque and flux all the SMPC strategies present the disadvantage of the variable frequency switching (f_{sw}). In particular, f_{sw} is practically random and depends only on the operating conditions of the electric drive. In fact, once the sampling time has been set, the only limit for f_{sw} that cannot be exceeded is $1/(2 \cdot T_s)$, therefore any f_{sw} between zero and $1/(2 \cdot T_s)$ is possible. This causes a high harmonic spectrum of the currents and voltages at the inverter output. Such a wide harmonic spectrum of currents and voltage increases the losses of the IM (and any other machine connected to the inverter), and also degrades the performance in terms of torque/speed ripple of the electric drive. Furthermore, the vector selected as a global optimum and used to supply the IM, is applied for the entire control period causing a high ripple on the controlled variables. In fact, in many cases there is no need to apply the vector for the entire control period so that the error of the controlled variable is canceled.

In the second part of this thesis the problems just described have been solved by implementing the modulation to the 2L-VSI. In particular, two modulation techniques have been studied and implemented. The modulation techniques are called two-vector modulation and three-vector modulation and have been implemented on the SMPC-FT3 strategy. The SMPC-FT3 strategy indicates a SMPC-type strategy in which in the first stage the flux (F) is controlled while in the second stage the torque (T) is controlled. In the second stage, are used only the three (3) voltage vectors that allowed to generate the smallest flux error this is why FT3 is placed at the end of the name.

Finally, the results obtained from the simulations for the SMPC-FT3 strategy without modulation and with the modulation technique called three vector modulation have also been validated experimental.

This thesis consists of six chapters. Chapter 1 presents the general theory on which the MPC control strategies are based, up to define the operating principle of SMPC strategies. Chapter 2 presents the main mathematical models used, including that of IM that of the flux observer and that of the inverter. In Chapter 3, all the mathematical relationships used for the prediction of the various quantities useful for implementing the SMPC strategies are illustrated and justified. Furthermore, a detailed analysis is carried out on the functioning of the SMPC strategies, presenting the re-

sults obtained from the simulations and identifying which strategies allow to control the IM. Chapter 4 presents the two different modulation techniques implemented on the SMPC-FT3 strategy, putting attention on the improvements obtained in terms of torque and current ripple reduction thanks to the introduction of the modulator. Chapter 5 presents the results obtained from the experimental tests conducted using the SMPC-FT3 strategy without modulator and with the three-vector modulation technique. The last chapter, Chapter 6, presents the conclusions and some suggestions for future research.

1
High-performance control for electric drives

The three-phase induction motor is one of the most used electric machines, thanks to its high reliability, low cost and robustness. At present, there are two strategies widely used in the field of electrical drives for AC motor. One is Field Oriented Control (FOC) [7]. FOC is a linear strategy, which uses linear controllers and a pulse width modulator (PWM) to generate the voltages applied to the motors. Thanks to the introduction of the FOC, it has been possible to use the induction machine (IM) in all those applications where DC motors were used, allowing the improvement of the reliability and robustness of the electric drives.

All the electric drives based on the FOC use the reference frame transformations to refer the three-phase quantities to a new two-phase orthogonal rotating reference frame. Using the system of differential equations defined in the new rotating reference system at an appropriate speed allows us to obtain the decoupling between flux and torque. Practically it is possible to control torque and flux using two different current commands. Therefore, thanks to the use of the FOC it was possible to control the IM in a similar way to the DC motor, avoiding all the typical problems of the DC motor and at the same time obtaining high dynamic performances.

However, FOC is based on a cascade structure, in which the external loop is responsible for the speed control, while the internal loop for the current control. In particular, both the external speed loop and the internal current loops use Proportional Integral (PI) controllers; and the PIs contain within them numerous parameters that must be carefully tuned in order to obtain good dynamic performance.

The seconds trategies widely used in the field of electrical drives for AC motor is the Direct Torque Control (DTC) [8]. The basic idea of the DTC is to use existing torque and flux errors to control the inverter, without using current loops, transformations and modulators. In particular, a predefined look up table (LUT) is used to select the switching vectors that allow to maintain the flux and torque errors within certain hysteresis bands. Therefore, it is possible to state that one of the major strengths of the DTC is the simplicity and low costs. However, the use of hysteresis comparators causes the variable switching frequency, depending on the parameters of the machine, the load conditions and the operating speed. This, generally causes a high harmonic distortion of the currents and a non-uniform distribution of

the switching losses in the switches. To solve this problem, numerous modulation techniques based on DTCs have been proposed [9, 10]. However, it is possible to state that all the proposed solutions and improvements always cause an increase in complexity and costs. In any case, at present, with the FOC and DTC it is possible to satisfy most industrial applications.

In recent years, thanks to the significantly higher microcontroller computational power, it has been possible to implement new control strategies including the Model Predictive Control (MPC), therefore at present, a possible alternative in the field of high performance drives is the MPC. The main feature of the MPC is to use the model of the system, in order to predict the future behavior of the variables to be controlled. In particular, the variables are predicted up to a predefined time horizon in order to select the optimal actuations, according to the established optimization criterion. Generally, the MPC is very easy to understand and to implement and the methodology is suitable to be modified and expanded based on needs [1].

The Model Predictive Control (MPC) technique is widely used in many industrial sectors and not only in the field of electric drives [1–3]. The first ideas of MPC were developed in the 1960s as an application of the theory of optimal control, the industrial interest in these ideas began at the end of the 1970s [1, 3]. The first applications of the MPC in power electronics/electrical drives, occurred at the beginning of 1980s, in high power systems with low switching frequency [4], since the use of high switching frequencies was not possible due to the high number of calculations necessary for the implementation of this strategy.

Only the strong development of microprocessors in recent years has increased the interest to apply the MPC in the industrial sector of electric drives and power electronic, allowing therefore to open new avenues of research in the field of high performance electrical drives.

In this chapter we will discuss the general theory on which the MPC is based will be briefly discussed. Furthermore, the operating principle of an electric drive based on the Finite Control Set-MPC (FCS-MPC) which is a particular variant of MPC will be analyzed, paying particular attention to the main problems of this control strategy. Finally, a new control strategy, called Sequential-MPC (SMPC) will be presented that will solve some of the FCS-MPC problems.

1.1 General theory of MPC

Model Predictive Control (MPC) refers to a wide family of control strategies and not to a specific control strategy [1]. All these strategies use the system model to predict the future behavior of the variables to be controlled until a predefined horizon in time. After having predicted the variables and known their reference, the optimal actuation is chosen so as to minimize the difference between the predicted value and the reference, which in this

field is commonly called cost function. These control strategies have many advantages, among which the most important are: ease of understanding, the possibility of applying them to numerous systems and the possibility of compensating the digital time typical of digital controls [11]. Among the main disadvantages there is certainly to consider the high number of calculations necessary to be able to apply this type of strategies and the need to have a precise model of the system in order to have good results. When the MPC strategy is applied, it is necessary:

- to use a model that allows at predicting the behavior of the variables until a horizon in time;
- to identify a cost function that describes the desired behavior of the system;
- to evaluate the cost function in order to choose the optimal actuations.

The model used for prediction is always a discrete model with the cost functions that can be of different types, but that in any case must be able to describe the error between reference and predicted variables. Among all the possibilities, the future actuations are chosen on the basis of the minimization of the error between reference and predicted variables, i.e. on the basis of the minimization of the cost function.

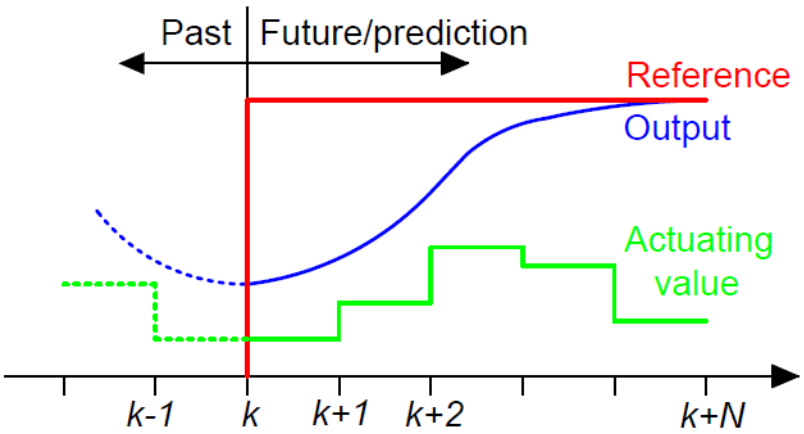

Figure 1.1: Operation of the MPC. Adapted from [12].

Fig.1.1 shows the operating principle of the MPC, the various time instants k are shown on the abscissa axis, the blue line identifies the system output, the red one the reference and finally the selected actuations are shown in green. At the present instant k all the information/model-measurements are available, from this information the outputs of the system are predicted for a fixed orizont N. In reality, N is always limited to one or

two sampling periods, in order to reduce the number of calculations necessary. In particular with $N = 2$ the digital control delay can be compensated. The sequence of the inputs is established proceeding with the minimization of a cost function, in this way is possible to reduce the error between the *reference* and the *predicted output*.

1.2 Electric drive based on the Finite Control Set Model Predictive Control (FCS-MPC)

As noted above, the MPC is widely used in many industrial sectors, and at present it is gaining more and more attention also in the field of electric drives. The possible types of electric drives based on the MPC are numerous [13], but in any case to date, among the most used strategies based on the MPC there is certainly the Finite Control Set-MPC (FCS-MPC). The FCS-MPC is a particular variant of MPC whose basic concept is to consider the discrete nature of the power converter, allowing an important simplification of the control strategy [14]. In fact, considering that the power switches, can only assume two states (ON or OFF), the number of possible states of the power converter S must be finite. Consequently, the cost function has to be evaluated only for a finite number of possible states applicable by the inverter.

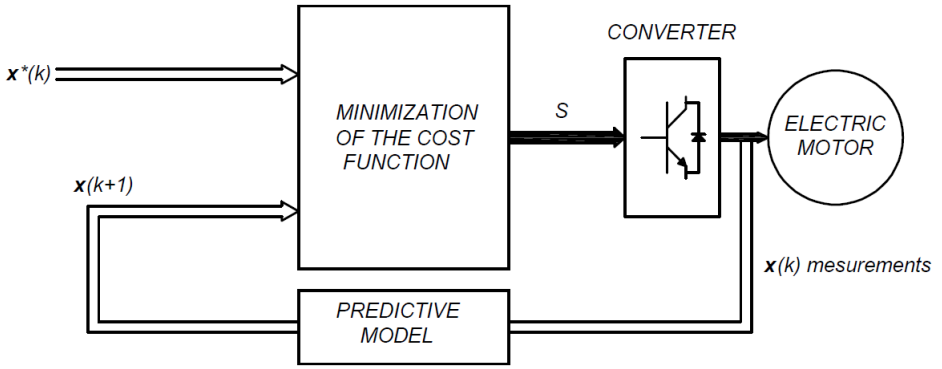

Figure 1.2: General MPC scheme for electrical drives.

In the block diagram shown in Fig.1.2, $\boldsymbol{x}(k)$ is the vector of measured variables at the current instant k, $\boldsymbol{x}(k+1)$ is the value of the controlled variables, at the instant $k+1$, $\boldsymbol{x}^*(k)$ is the reference imposed for the controlled variables, while S is the state of the inverter. At the instant k starting from $\boldsymbol{x}(k)$, using the model it is possible to calculate $\boldsymbol{x}(k+1)$ knowing all the possible inverter states. The state selected S is the one that allows to minimize the cost function, i.e. the error between $\boldsymbol{x}^*(k)$ and $\boldsymbol{x}(k+1)$.

One of the main problems of the FCS-MPC is related to the definition of weighting factors within the cost function. In fact, using a single cost

function with variables of different nature and different order of magnitude inside, it is essential to use weighting factors. The calculation of weighting factors is one of the greatest challenges when implementing such strategies, given that they have an important influence on performance of the control. Moreover, they are often defined by iterative processes that are not accepted by many users [15–17]. To solve these problems, a new control strategy called sequential MPC (SMPC) has been recently proposed and applied to an induction machine.

1.3 Electric drive for induction machine based on the sequential MPC (SMPC)

Until now, the FCS-MPC of torque and flux of AC machines has been implemented using a single cost function and using a weighting factor to give more or less importance to the minimization of torque or flux error [5, 6]. As already noted above, the calculation of the weighting factor is one of the main problems in this control strategy. One of the proposed solutions for predictive torque and flux control for AC machine that does not use weighting factors is the Sequential Model Predictive Control (SMPC) [18], based on a two-stage sequential structure with a single cost function for each stage. This strategy, in the first stage controls the torque and the second stage controls the flux, and a two-level Voltage Source Inverter (2L-VSI) is used to supply the induction motor. In particular, in the SMPC strategy [18], the first cost function is evaluated for all seven available voltage vectors, then the two voltage vectors that generate the smallest torque error are selected for the evaluation of the flux error. Finally, between the available two voltage vectors, the voltage vector that minimizes the flux error is selected as global optimal and applied through the inverter.

At this point, it is important to identify the general concept behind this control strategy. The general concept, is that there is the possibility not to use the weighting factors and therefore to avoid all the associated tuning work. To do this, it is sufficient to carry out a sequential evaluation of the cost functions in several stages, reducing to each stage the number of vectors that can be used for the evaluation of the cost function defined in the next stage, up to define the optimal voltage vector to selected and to apply at the electric motor.

1.3.1 Design of a control based on the SMPC

For the design of an electrical drive based on the SMPC it is essential:

- to model the power converter considering its discrete nature according to the type of converter;

- to define the number of stages and the cost functions that allow to describe the desired behavior of the system;
- to build a discrete model of the electric motor that allows at predicting the behavior of the variables to be controlled.

Finally we observe that for the construction of the discrete model, in general the Euler method is used, as it is the simplest way to discretize systems of the first order. Using this method, the derivative is approximated using the following equation:

$$\frac{dx}{dt} = \frac{x(k+1) - x(k)}{T_s} \tag{1.1}$$

where T_s is the sampling time.

As one of the main objectives of this thesis is the study of all possible SMPC techniques that use two different control stages applied to an induction motor, in the following chapter the main mathematical models necessary for the study will be obtained.

2
Matematical models

The three-phase induction motor (IM) is one of the most used electric motors in the industrial field. In fact, the IM was born to work directly connected to the electric network without the use of converters, but obviously with low dynamic performance. However, over the years thanks to the strong development of the power electronics for the development of reliable inverters, numerous control strategies have been studied and implemented with the aim of increasing the dynamic performance obtainable by induction motors. At present the Field Oriented Control (FOC) and the Direct Torque Control (DTC) are among the most used strategies in electric drives. But, the need to have more and more high dynamic performance by using strategies that at the same time require little tuning work, has pushed the research to the study of new control strategies including the SMPC strategy.

As already noted above for the study and implementation of an electric drive that use a SMPC strategy, it is essential to derive the discrete model of the electric motor and that of the inverter. Therefore, in this chapter the mathematical models of the IM and of the inverter necessary for the implementation of SMPC strategies will be obtained. Furthermore, using the motor equations, the implemented observer model will also be obtained, used in these control strategies with the aim of improving their robustness.

In particular, for the induction machine, the two-phase model is obtained which generally allows a considerable simplification of the model. The most employed two-phase models are the ones in the fixed stator reference frame ($\alpha\beta$) or the one in the rotating synchronous reference frame with the rotor flux (dq). In particular, for the implementation of the SMPC strategy implemented in this thesis the two-phase model in the stator reference frame ($\alpha\beta$) is used. Using the induction motor equations defined in the different reference frame, the flux observer model $VI\theta$ is then derived. Finally it is presented the matematical model of the three-phase useful for identifying its discrete nature from which the SMPC takes advantage.

2.1 Mathematical models of the three-phase induction machine

In this section the mathematical model of the three-phase induction motor is obtained more detailed description can be found in [19–21]. The induction

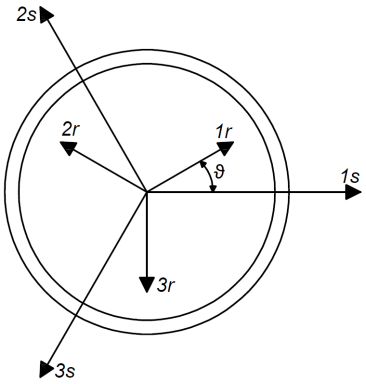

Figure 2.1: Axes of magnetic symmetry of stator $(1s, 2s, 3s)$ and rotor $(1r, 2r, 3r)$, for a three-phase induction machine, with θ that indicate the angle between the two reference frames.

motor model is obtained for a three-phase machine with a pole-pair number $p = 1$, under the following assumptions:

- the same stator and rotor turns;
- absence of magnetic saturation;
- sinusoidal distribution winding;
- constant air gap.

In Fig.2.1 the fixed stator reference frame $(1s, 2s, 3s)$ and the rotating rotor reference frame $(1r, 2r, 3r)$ are shown, with θ is indicated the generic angle between the two reference frames.

The electrical and magnetic equations of stator can be organized in vectorial form. Therefore the vector of stator voltage $\boldsymbol{V}_s^{123}$, the vector of stator current $\boldsymbol{I}_s^{123}$ and the vector of stator flux linkages $\boldsymbol{\Lambda}_s^{123}$ are defined:

$$\boldsymbol{V}_s^{123} = \begin{pmatrix} v_{s1} \\ v_{s2} \\ v_{s3} \end{pmatrix} \qquad \boldsymbol{I}_s^{123} = \begin{pmatrix} i_{s1} \\ i_{s2} \\ i_{s3} \end{pmatrix} \qquad \boldsymbol{\Lambda}_s^{123} = \begin{pmatrix} \lambda_{s1} \\ \lambda_{s2} \\ \lambda_{s3} \end{pmatrix} \tag{2.1}$$

where the components of these three vectors represent the instantaneous values of voltage, current and flux linkages, of the three windings at the stator.

The electric and magnetic rotor equations can also be organized in the same way, using the vector of rotor voltage $\boldsymbol{V}_r^{123}$, the vector of rotor current $\boldsymbol{I}_r^{123}$ and the vector of rotor flux $\boldsymbol{\Lambda}_r^{123}$ defined as:

$$\boldsymbol{V}_r^{123} = \begin{pmatrix} v_{r1} \\ v_{r2} \\ v_{r3} \end{pmatrix} \qquad \boldsymbol{I}_r^{123} = \begin{pmatrix} i_{r1} \\ i_{r2} \\ i_{r3} \end{pmatrix} \qquad \boldsymbol{\Lambda}_r^{123} = \begin{pmatrix} \lambda_{r1} \\ \lambda_{r2} \\ \lambda_{r3} \end{pmatrix} \tag{2.2}$$

where the components of these three vectors represent the instantaneous values of voltage, current and flux linkages, of the equivalent three-phase rotor winding.

It can be observed how the rotor equations refer to an equivalent three-phase winding, in fact the rotor structure is generally polyphase. In any case, a polyphase winding can always be studied using a three-phase equivalent winding [22].

Using the stator and rotor vectors, defined in equations (2.1) and (2.2), it is possible to define the electrical (2.3) and magnetic (2.4) equations of the induction machine as follows:

$$\begin{cases} \boldsymbol{V}_s^{123} = \boldsymbol{R}_s^{123}\boldsymbol{I}_s^{123} + \frac{d\boldsymbol{\Lambda}_s^{123}}{dt} \\ \boldsymbol{V}_r^{123} = \boldsymbol{R}_r^{123}\boldsymbol{I}_r^{123} + \frac{d\boldsymbol{\Lambda}_r^{123}}{dt} \end{cases} \tag{2.3}$$

$$\begin{cases} \boldsymbol{\Lambda}_s^{123} = \boldsymbol{L}_\sigma^s\boldsymbol{I}_s^{123} + \boldsymbol{M}_{123}^{ss}\boldsymbol{I}_s^{123} + \boldsymbol{M}_{123}^{sr}\boldsymbol{I}_r^{123} \\ \boldsymbol{\Lambda}_r^{123} = \boldsymbol{L}_\sigma^r\boldsymbol{I}_r^{123} + \boldsymbol{M}_{123}^{rr}\boldsymbol{I}_r^{123} + \boldsymbol{M}_{123}^{rs}\boldsymbol{I}_s^{123} \end{cases} \tag{2.4}$$

All matrices from in the equations (2.3) and (2.4) are 3x3 matrices. In particular, $\boldsymbol{R}_s^{123}$ and $\boldsymbol{R}_r^{123}$ contain the values of the stator resistance and equivalent rotor resistance, while $\boldsymbol{L}_\sigma^s$ and $\boldsymbol{L}_\sigma^r$ are the stator leakage inductance and the equivalent rotor leakage inductance. Their expressions are shown below:

$$\boldsymbol{R}_s^{123} = R_s\begin{pmatrix}1&0&0\\0&1&0\\0&0&1\end{pmatrix} \qquad \boldsymbol{R}_r^{123} = R_r\begin{pmatrix}1&0&0\\0&1&0\\0&0&1\end{pmatrix} \tag{2.5}$$

$$\boldsymbol{L}_\sigma^s = L_\sigma^s\begin{pmatrix}1&0&0\\0&1&0\\0&0&1\end{pmatrix} \qquad \boldsymbol{L}_\sigma^r = L_\sigma^r\begin{pmatrix}1&0&0\\0&1&0\\0&0&1\end{pmatrix} \tag{2.6}$$

Finally, $\boldsymbol{M}_{123}^{ss}$ and $\boldsymbol{M}_{123}^{rr}$ are stator self-coupling matrices, while $\boldsymbol{M}_{123}^{sr}$ and $\boldsymbol{M}_{123}^{rs}$ are the matrices of mutual coupling stator-rotor. Thanks to the initial hypotheses, $\boldsymbol{M}_{123}^{ss}$ and $\boldsymbol{M}_{123}^{rr}$ have only constant terms, while the terms of $\boldsymbol{M}_{123}^{sr}$ and $\boldsymbol{M}_{123}^{rs}$ are a function of the relative position between stator and rotor identified by θ and moreover they consider that the windings are shifted by 120° electrical. Their expressions are shown below:

$$\boldsymbol{M}_{123}^{ss} = M\begin{pmatrix}1&-1/2&-1/2\\-1/2&1&-1/2\\-1/2&-1/2&1\end{pmatrix} \tag{2.7}$$

$$\boldsymbol{M}_{123}^{rr} = M\begin{pmatrix}1&-1/2&-1/2\\-1/2&1&-1/2\\-1/2&-1/2&1\end{pmatrix} \tag{2.8}$$

$$\boldsymbol{M}_{123}^{sr} = M \begin{pmatrix} cos(\theta) & cos(\theta + 2\pi/3) & cos(\theta + 4\pi/3) \\ cos(\theta + 4\pi/3) & cos(\theta) & cos(\theta + 2\pi/3) \\ cos(\theta + 2\pi/3) & cos(\theta + 4\pi/3) & cos(\theta) \end{pmatrix} \tag{2.9}$$

$$\boldsymbol{M}_{123}^{rs} = M \begin{pmatrix} cos(\theta) & cos(\theta + 4\pi/3) & cos(\theta + 2\pi/3) \\ cos(\theta + 2\pi/3) & cos(\theta) & cos(\theta + 4\pi/3) \\ cos(\theta + 4\pi/3) & cos(\theta + 2\pi/3) & cos(\theta) \end{pmatrix} \tag{2.10}$$

with M that it is possible to calculate as shown in the equation (2.11), note the number of turns of the stator and rotor winding N and the reluctance to the air gap $\Re_t$.

$$M = \frac{NN}{\Re_t} \tag{2.11}$$

It is possible to observe how the matrices reported in (2.5) and (2.6) are identity matrices multiplied by the costant values. Consequently the electric and magnetic equations can be rewritten as follows:

$$\begin{cases} \boldsymbol{V}_s^{123} = R_s \boldsymbol{I}_s^{123} + \frac{d\boldsymbol{\Lambda}_s^{123}}{dt} \\ \boldsymbol{V}_r^{123} = R_r \boldsymbol{I}_r^{123} + \frac{d\boldsymbol{\Lambda}_r^{123}}{dt} \end{cases} \tag{2.12}$$

$$\begin{cases} \boldsymbol{\Lambda}_s^{123} = L_\sigma^s \boldsymbol{I}_s^{123} + \boldsymbol{M}_{123}^{ss} \boldsymbol{I}_s^{123} + \boldsymbol{M}_{123}^{sr} \boldsymbol{I}_r^{123} \\ \boldsymbol{\Lambda}_r^{123} = L_\sigma^r \boldsymbol{I}_r^{123} + \boldsymbol{M}_{123}^{rr} \boldsymbol{I}_r^{123} + \boldsymbol{M}_{123}^{rs} \boldsymbol{I}_s^{123} \end{cases} \tag{2.13}$$

In conclusion, the three-phase mathematical model of the induction machine consists of six equations of the first order, where the rotor equations are valid in the rotating three-phase rotor reference frame $(1r, 2r, 3r)$, while the stator equations in the fixed three-phase stator reference frame $(1s, 2s, 3s)$.

Below we will briefly explain the procedure for to obtain a model of the machine described by only four equations, in other words the concept of an equivalent two-phase machine will be introduced. More details are faund in [19, 20].

2.2 Two-phase model of the induction machine

The introduction of the two-phase equivalent model allows to greatly simplify of the equations that describe the dynamic model of the three-phase machine, and it is widely used in the field of electric drives. To do this it is necessary to introduce two transformations; these transformations are commonly called transformations of the controllers and are B' and B:

$$\boldsymbol{B'} = \frac{2}{3} \begin{pmatrix} 1 & -1/2 & -1/2 \\ 0 & \sqrt{3}/2 & -\sqrt{3}/2 \end{pmatrix} \tag{2.14}$$

$$\boldsymbol{B} = \begin{pmatrix} 1 & 0 \\ -1/2 & \sqrt{3}/2 \\ -1/2 & \sqrt{3}/2 \end{pmatrix} \tag{2.15}$$

By using the transformation (2.14) it is possible to define the equations in the three-phase fixed reference frame $(1s, 2s, 3s)$ in the new two-phase fixed reference frame $(\alpha\beta)$, or define the equations in the three-phase rotating reference frame $(1r, 2r, 3r)$ in the new two-phase rotating reference frame synchronous with the rotor $(\alpha_r\beta_r)$, the same speech, but on the contrary it is valid for the transformation (2.15). In other words the transformation B allows to pass from the three-phase model of the induction machine to the two-phase model, while the transformation B' performs the inverse operation.

Therefore, if both members of the electrical equations (2.12) are multiplied by the transformation matrix B', it is possible to demostrate that this operation returns the equations illustrated in (2.16), that are the electrical equations of the equivalent two-phase machine.

$$\begin{cases} \boldsymbol{v}_{s\alpha\beta} = R_s \boldsymbol{i}_{s\alpha\beta} + \frac{d\boldsymbol{\lambda}_{s\alpha\beta}}{dt} \\ \boldsymbol{v}_{r\alpha\beta} = R_r \boldsymbol{i}_{r\alpha\beta} + \frac{d\boldsymbol{\lambda}_{r\alpha\beta}}{dt} \end{cases} \tag{2.16}$$

All vectors quantities of the electrical equations (2.16) are two-component, and each of the two electrical equations is valid in its own reference frame. In other words, the stator and rotor equations are both two-phase, but they are referred at two different reference frames. In particular, the stator equations are valid in a fixed reference frame $(\alpha\beta)$, while the rotor equations are valid in a rotary synchronous reference frame with the rotor $(\alpha_r\beta_r)$.

For the magnetic equations it is possible to adopt the same procedure, but in this case we must keep in mind that the product between matrices is not commutative. To work around this problem, is necessary to use also the inverse transformation B. To clarify what has just been said, the intermediate step is shown in the equation (2.17) before obtaining the two-phase magnetic equations in $(\alpha\beta)$ and $(\alpha_r\beta_r)$.

$$\begin{cases} \boldsymbol{B'\Lambda}_s^{123} = L_\sigma^s \boldsymbol{B'I}_s^{123} + \boldsymbol{B'M}_{123}^{ss}(\boldsymbol{BI}_s^{\alpha\beta}) + \boldsymbol{B'M}_{123}^{sr}(\boldsymbol{BI}_r^{\alpha\beta}) \\ \boldsymbol{B'\Lambda}_r^{123} = L_\sigma^r \boldsymbol{B'I}_r^{123} + \boldsymbol{B'M}_{123}^{rr}(\boldsymbol{BI}_r^{\alpha\beta}) + \boldsymbol{B'M}_{123}^{rs}(\boldsymbol{BI}_s^{\alpha\beta}) \end{cases} \tag{2.17}$$

Performing the steps we have that:

$$\boldsymbol{B'M}_{123}^{ss}\boldsymbol{B} = \boldsymbol{B'M}_{123}^{rr}\boldsymbol{B} = \frac{3}{2}M \begin{pmatrix} 1 & 0 \\ 0 & 1 \end{pmatrix} \tag{2.18}$$

$$\boldsymbol{B'M}_{123}^{sr}\boldsymbol{B} = \frac{3}{2}M \begin{pmatrix} cos(\theta) & -sin(\theta) \\ sin(\theta) & cos(\theta) \end{pmatrix} \tag{2.19}$$

$$\boldsymbol{B'M}_{123}^{rs}\boldsymbol{B} = \frac{3}{2}M \begin{pmatrix} cos(\theta) & sin(\theta) \\ -sin(\theta) & cos(\theta) \end{pmatrix} \tag{2.20}$$

We define now:

$$L_m = \frac{3}{2}M \begin{pmatrix} 1 & 0 \\ 0 & 1 \end{pmatrix} \tag{2.21}$$

$$A^T(\theta) = \begin{pmatrix} cos(\theta) & -sin(\theta) \\ sin(\theta) & cos(\theta) \end{pmatrix} \tag{2.22}$$

$$A(\theta) = \begin{pmatrix} cos(\theta) & sin(\theta) \\ -sin(\theta) & cos(\theta) \end{pmatrix} \tag{2.23}$$

where L_m is the mutual inductance for the two-phase equivalent machine, $A^T(\theta)$ and $A(\theta)$ are two matrix that allow to describe the dependence of mutual couplings from θ. Also in this case the equation of the stator flux is valid only in the $(\alpha\beta)$ reference frame, while the equation of the rotor flux is valid only $(\alpha_r\beta_r)$ reference frame.

Using the expressions shown in the equations (2.21),(2.22) and (2.23) it is possibile to rewrite the magnetic equations in (2.17) as shown below:

$$\begin{cases} \boldsymbol{\lambda}_{s\alpha\beta} = L_{\sigma s}\boldsymbol{i}_{s\alpha\beta} + L_m\boldsymbol{i}_{s\alpha\beta} + L_m\boldsymbol{A}^T(\theta)\boldsymbol{i}_{r\alpha\beta} \\ \boldsymbol{\lambda}_{r\alpha\beta} = L_{\sigma r}\boldsymbol{i}_{r\alpha\beta} + L_m\boldsymbol{i}_{r\alpha\beta} + L_m\boldsymbol{A}(\theta)\boldsymbol{i}_{s\alpha\beta} \end{cases} \tag{2.24}$$

The equations just obtained can be further simplified by introducing the *stator inductance* L_s and the *rotor inductance* L_r, defined as follow:

$$\begin{cases} L_s = L_{\sigma s} + L_m \\ L_r = L_{\sigma r} + L_m \end{cases} \tag{2.25}$$

It is important to remember that L_s and L_r are not true phase inductances because they contain the term of mutual inductance, but by exploiting the definition of these two new inductance, it is possible to define the magnetic model of the induction machine in a very compact way:

$$\begin{cases} \boldsymbol{\lambda}_{s\alpha\beta} = L_s\boldsymbol{i}_{s\alpha\beta} + L_m\boldsymbol{A}^T(\theta)\boldsymbol{i}_{r\alpha\beta} \\ \boldsymbol{\lambda}_{r\alpha\beta} = L_m\boldsymbol{A}(\theta)\boldsymbol{i}_{s\alpha\beta} + L_r\boldsymbol{i}_{r\alpha\beta} \end{cases} \tag{2.26}$$

The following are the electrical and magnetic equations of the two-phase model of the induction machine:

$$\begin{cases} \boldsymbol{v}_{s\alpha\beta} = R_s\boldsymbol{i}_{s\alpha\beta} + \frac{d\boldsymbol{\lambda}_{s\alpha\beta}}{dt} \\ \boldsymbol{v}_{r\alpha\beta} = R_r\boldsymbol{i}_{r\alpha\beta} + \frac{d\boldsymbol{\lambda}_{r\alpha\beta}}{dt} \end{cases} \tag{2.27}$$

$$\begin{cases} \boldsymbol{\lambda}_{s\alpha\beta} = L_s\boldsymbol{i}_{s\alpha\beta} + L_m\boldsymbol{A}^T(\theta)\boldsymbol{i}_{r\alpha\beta} \\ \boldsymbol{\lambda}_{r\alpha\beta} = L_m\boldsymbol{A}(\theta)\boldsymbol{i}_{s\alpha\beta} + L_r\boldsymbol{i}_{r\alpha\beta} \end{cases} \tag{2.28}$$

At this point, the goal is to be able to define all the equations in the same reference frame, in order to obtain a model that is actually easy to interpret and use. This operation will be done in the next section, where in fact all the equations are defined in the rotating reference frame $(\alpha_k\beta_k)$.

2.2.1 Two-phase model of the induction machine in a generic rotating reference frame ($\alpha_k\beta_k$)

To define a model that is effectively usable, it is essential to refer equations (2.27) and (2.28) to a single reference frame. This reference frame choose is $(\alpha_k\beta_k)$ that rotates at the generic speed ω_k.

Fig.2.2 shows in detail the fixed reference frame of stator $(\alpha\beta)$, the rotary reference frame of rotor $(\alpha_r\beta_r)$ at the rotor speed ω and the rotating reference frame at genric speed ω_k $(\alpha_k\beta_k)$ on which we want to define all the equations, moreover θ_k and θ indicate the relative angles present between the reference frames.

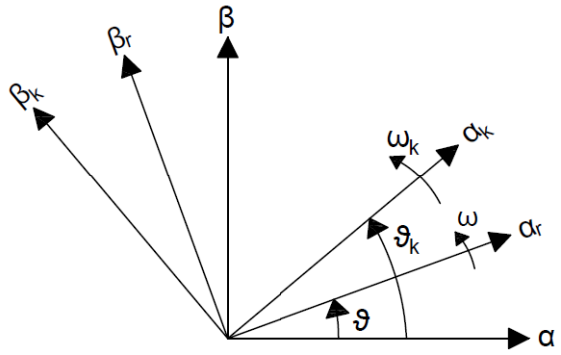

Figure 2.2: Stator fixed reference frame $(\alpha_s\beta_s)$, rotor rotary reference frame $(\alpha_r\beta_r)$ at the rotor speed (ω) with a phase shift of θ from $(\alpha_s\beta_s)$ and generic rotary reference frame $(\alpha_k\beta_k)$ at speed (ω_k) with a phase shift of θ_k from $(\alpha_s\beta_s)$.

Now, it is important to observe how the matrices $\boldsymbol{A}^T(\theta)$ and $\boldsymbol{A}(\theta)$ that describe the dependence of the mutual couplings from the rotor position, in (2.27) and (2.28). These matrices rapresent rotational's transformations. In particular $\boldsymbol{A}^T(\theta)$ allows to define the spatial vectors defined in the rotor raference frame $(\alpha_r\beta_r)$, in the reference frame $(\alpha\beta)$. At same way, $\boldsymbol{A}(\theta)$ allows to define the spatial vectors defined in the raference frame $(\alpha\beta)$, in the reference frame $(\alpha_r\beta_r)$. The rotational transformation can also be expressed using a complex operators, as follows:

- $\boldsymbol{A}^T(\theta) \rightarrow \mathrm{e}^{j\theta}$ allow the transition from: $(\alpha_r\beta_r)$ to $(\alpha\beta)$
- $\boldsymbol{A}(\theta) \rightarrow \mathrm{e}^{-j\theta}$ allow the transition from: $(\alpha\beta)$ to $(\alpha_r\beta_r)$

It is also possible to define the matrix and the corresponding complex operators that allow at defining the spatial vectors defined in the reference frame $(\alpha\beta)$ or $(\alpha_r\beta_r)$, or $(\alpha_k\beta_k)$. They are:

- $\boldsymbol{A}^T(\theta_k) \rightarrow \mathrm{e}^{j\theta_k}$ allow the transition from: $(\alpha\beta)$ to $(\alpha_k\beta_k)$
- $\boldsymbol{A}(\theta_k) \rightarrow \mathrm{e}^{-j\theta_k}$ allow the transition from: $(\alpha_k\beta_k)$ to $(\alpha\beta)$

- $\boldsymbol{A}^T(\theta_k - \theta) \rightarrow \mathrm{e}^{j(\theta_k-\theta)}$ allow the transition from: $(\alpha_r\beta_r)$ to $(\alpha_k\beta_k)$
- $\boldsymbol{A}(\theta_k - \theta) \rightarrow \mathrm{e}^{-j(\theta_k-\theta)}$ allow the transition from: $(\alpha_k\beta_k)$ to $(\alpha_r\beta_r)$

The just defined transformations can easily be obtained by observing Fig.2.2.

Using the matrices/complex operators just illustrated, it is possible to define the two-phase model of the induction machine in the reference frame $(\alpha_k\beta_k)$. For reasons of clarity and simplicity of the steps, the complex operators will be used. So using the complex operators the magnetic equations (2.28) can be rewritten as:

$$\begin{cases} \boldsymbol{\lambda}_{s\alpha\beta} = L_s \boldsymbol{i}_{s\alpha\beta} + L_m \mathrm{e}^{j\theta} \boldsymbol{i}_{r\alpha\beta} \\ \boldsymbol{\lambda}_{r\alpha\beta} = L_m \mathrm{e}^{-j\theta} \boldsymbol{i}_{s\alpha\beta} + L_r \boldsymbol{i}_{r\alpha\beta} \end{cases} \tag{2.29}$$

Below are shown only the main steps to report the stator magnetic equations defined in the reference frame $(\alpha\beta)$ in the reference frame $(\alpha_k\beta_k)$, a more detailed description can be found in [20].

In order to obtain the magnetic stator equations in the reference frame $(\alpha_k\beta_k)$, it is sufficient to multiply both members of the equation for the complex operator $\mathrm{e}^{-j\theta_k}$, as shown below:

$$\mathrm{e}^{-j\theta_k} \boldsymbol{\lambda}_{s\alpha\beta} = L_s \mathrm{e}^{-j\theta_k} \boldsymbol{i}_{s\alpha\beta} + L_m \mathrm{e}^{-j\theta_k} \mathrm{e}^{j\theta} \boldsymbol{i}_{r\alpha\beta} \tag{2.30}$$

from which it is obtained:

$$\boldsymbol{\lambda}_{s\alpha\beta k} = L_s \boldsymbol{i}_{s\alpha\beta k} + L_m \boldsymbol{i}_{r\alpha\beta k} \tag{2.31}$$

where $\boldsymbol{\lambda}_{s\alpha\beta k}$, $\boldsymbol{i}_{s\alpha\beta k}$ and $\boldsymbol{i}_{r\alpha\beta k}$ are respectively the stator flux, the stator current and the rotor current all referred to the new rotary reference frame $(\alpha_k\beta_k)$. With the same procedure and using the complex operators defined above, all the electrical and magnetic equations can be referred at the reference frame $(\alpha_k\beta_k)$.

The following are the electrical and magnetic equations, obtainable by executing all the steps, which describe the model of the two-phase induction machine in the reference frame $(\alpha_k\beta_k)$.

$$\begin{cases} \boldsymbol{v}_{s\alpha\beta k} = R_s \boldsymbol{i}_{s\alpha\beta k} + \frac{d\boldsymbol{\lambda}_{s\alpha\beta k}}{dt} + j\omega_k \boldsymbol{\lambda}_{s\alpha\beta k} \\ \boldsymbol{v}_{r\alpha\beta k} = R_r \boldsymbol{i}_{r\alpha\beta k} + \frac{d\boldsymbol{\lambda}_{r\alpha\beta k}}{dt} + j(\omega_k - \omega) \boldsymbol{\lambda}_{r\alpha\beta k} \end{cases} \tag{2.32}$$

$$\begin{cases} \boldsymbol{\lambda}_{s\alpha\beta k} = L_s \boldsymbol{i}_{s\alpha\beta k} + L_m \boldsymbol{i}_{r\alpha\beta k} \\ \boldsymbol{\lambda}_{r\alpha\beta k} = L_m \boldsymbol{i}_{s\alpha\beta k} + L_r \boldsymbol{i}_{r\alpha\beta k} \end{cases} \tag{2.33}$$

with ω that is the electric rotation speed of the rotor.

As previously noted for the implementation of the Sequential Model Predictive Control (SMPC) for induction machine, the model in the reference frame $(\alpha\beta)$ is used, it will be obtained in the next section, and moreover it will be completed introducing the expression of torque and the mechanical equation of the machine.

2.2.2 Complete model of the induction machine in frame ($\alpha\beta$)

The model described by equations (2.32) and (2.33) is a quite general model, in fact no particular hypothesis has been made on the rotating reference frame ($\alpha_k\beta_k$). To get the electrical equations and magnetic equations in the reference frame ($\alpha\beta$), it is enough to impose $\omega_k = 0$, in this way practically the coincidence between the reference frame ($\alpha_k\beta_k$) and that ($\alpha\beta$) is imposed. Furthermore, it must be considered that during the operation of the machine, the rotor winding shorted, consequently $\boldsymbol{v}_{\alpha\beta kr} = \mathbf{0}$. In this way starting from equations (2.32) and (2.33), it is possible to obtain the equations of the induction machine in the reference frame ($\alpha\beta$), that are:

$$\begin{cases} \boldsymbol{v_s} = R_s \boldsymbol{i_s} + \frac{d\boldsymbol{\lambda_s}}{dt} \\ \mathbf{0} = R_r \boldsymbol{i_r} + \frac{d\boldsymbol{\lambda_r}}{dt} - j\omega \boldsymbol{\lambda_r} \end{cases} \tag{2.34}$$

$$\begin{cases} \boldsymbol{\lambda_s} = L_s \boldsymbol{i_s} + L_m \boldsymbol{i_r} \\ \boldsymbol{\lambda_r} = L_m \boldsymbol{i_s} + L_r \boldsymbol{i_r} \end{cases} \tag{2.35}$$

where all the subscripts related to the reference frame have been eliminated, and with the following nomenclature the quantities in the reference frame ($\alpha\beta$) will always be indicated.

In order to obtain a complete dynamic model of the induction motor it is necessary to define the torque as a function of the magnetic and electrical quantities, which can be obtained by multiplying scalary the voltages on the two stator and the rotor windings, of the two-phase equivalent machine, for the respective currents $\boldsymbol{i_s}$ and $\boldsymbol{i_r}$:

$$\begin{cases} \boldsymbol{i_s} \times \boldsymbol{v_s} = \boldsymbol{i_s} \times R_s \boldsymbol{i_s} + \boldsymbol{i_s} \times \frac{d\boldsymbol{\lambda_s}}{dt} \\ \boldsymbol{i_r} \times \mathbf{0} = \boldsymbol{i_r} \times R_r \boldsymbol{i_r} + \boldsymbol{i_r} \times \frac{d\boldsymbol{\lambda_r}}{dt} + \boldsymbol{i_r} \times (-j\omega \boldsymbol{\lambda_r}) \end{cases} \tag{2.36}$$

where $\times$ is the scalar product.

The first term on the left of the equations system (2.36) is the electric power entering the system, the second term represents the Joule losses of the machine, the third term is the variation of magnetic energy over time, having neglected the losses in the iron in the model of the machine, the fourth term can only be the mechanical power delivered by the machine to less than a factor 3/2 that must be considered on the basis of the used transformations. Therefore the mechanical power P delivered by the machine is:

$$P = T\omega_r = \frac{3}{2} \boldsymbol{i_r} \times (-j\omega \boldsymbol{\lambda_r}) \tag{2.37}$$

with ω_r that is the mechanical speed of the machine and it is related to the electric rotor pulsation, from the known relation $\omega = p\omega_r$, and T is the mechanical torque. Using the relationship that binds the electrical pulsation

to the mechanical one, it is possible to derive the expression of the torque supplied by the induction motor:

$$T = \frac{3}{2} p \boldsymbol{i_r} \times (-j \boldsymbol{\lambda_r}) = \frac{3}{2} p \boldsymbol{i_r} \wedge \boldsymbol{\lambda_r} \tag{2.38}$$

where $\wedge$ is the vector product. In the field of electric drives, it is preferred to use other torque expressions employing the stator current $\boldsymbol{i_s}$, since it is actually measurable in contrast to the rotor current $\boldsymbol{i_r}$.

Using equations (2.35), it is possible to obtain the desired torque expression starting from (2.38). The following are shown the main steps.

$$T = \frac{3}{2} p \boldsymbol{i_r} \wedge (L_r \boldsymbol{i_r} + M \boldsymbol{i_s}) = \frac{3}{2} p (\boldsymbol{i_r} \wedge M \boldsymbol{i_s}) = \frac{3}{2} p (\frac{\boldsymbol{\lambda_s} - L_s \boldsymbol{i_s}}{M}) \wedge (M \boldsymbol{i_s}) \tag{2.39}$$

Finally, from the equation (2.39) it is possible to obtain the torque expression as a function of the flux $\boldsymbol{\lambda_s}$ and current $\boldsymbol{i_s}$ stator, thus eliminating the dependence on the rotor current $\boldsymbol{i_r}$.

$$T = \frac{3}{2} p \boldsymbol{\lambda_s} \wedge \boldsymbol{i_s} \tag{2.40}$$

To complete the dynamic model of the machine, the mechanical equation of the machine needs to be added:

$$T - T_L = J \frac{d\omega_r}{dt} \tag{2.41}$$

where T_L is the load torque, J the moment of inertia and ω_r the mechanical rotation speed.

The equations that allow to describe the dynamic model of the induction machine in the fixed stator reference frame ($\alpha\beta$) are shown below

$$\boldsymbol{v_s} = R_s \boldsymbol{i_s} + \frac{d\boldsymbol{\lambda_s}}{dt} \tag{2.42}$$

$$\boldsymbol{0} = R_r \boldsymbol{i_r} + \frac{d\boldsymbol{\lambda_r}}{dt} - j\omega \boldsymbol{\lambda_r} \tag{2.43}$$

$$\boldsymbol{\lambda_s} = L_s \boldsymbol{i_s} + L_m \boldsymbol{i_r} \tag{2.44}$$

$$\boldsymbol{\lambda_r} = L_m \boldsymbol{i_s} + L_r \boldsymbol{i_r} \tag{2.45}$$

$$T = \frac{3}{2} p \boldsymbol{\lambda_s} \wedge \boldsymbol{i_s} \tag{2.46}$$

$$T - T_L = J \frac{d\omega_r}{dt} \tag{2.47}$$

Tab.2.1 the parameters and their values of the induction machine used, while in Tab.2.2 its nameplate data are shown.

Table 2.1: Parametrers of the used induction machine.

Machine parametres	Value
R_s	0.4 Ω
R_r	0.31 Ω
L_s	33.779 mH
L_r	97.6 mH
L_m	97.6 mH
J	0.062 $kg \cdot m^2$
p	2

Table 2.2: Nameplate of the used induction machine.

Machine nameplate	Value
Rated power P_n	7.5 kW
Rated voltage V_n	400 V
Rated current I_f	17 A_{rms}
Rated speed ω_n	1460 rpm

2.3 Observers and estimetors

In the field of controls, estimators and observers are often used. They use the system model to calculate the value of some quantities that do not want or can not be measured, starting from other quantities. The feature of the estimator is to work in open loop, while that of the observers is to work in close loop. So it is possible to state that the observers are generally more robust and allow to define quantities more accurately. The common critical issues of observers and estimators is the estimation of parameters that are not constant and dependent on other quantities.

In electric drives for induction motors that use FOC strategy, observers and estimators of the flux are often used. In this thesis, although not having used a FOC strategy, a flux observer was used to calculate the magnitude of the stator flux. The observer used in this thesis is commonly called $VI\theta$ and it can be obtained by combining two estimators. The two flux estimators used, are communly called VI and $I\theta$, their models are presented below, before to present the stator flux observer useful for this work.

2.3.1 The VI flux estimetor

The VI estimator (VI) use the stator current $\boldsymbol{i_s}$ and the stator voltage $\boldsymbol{v_s}$, defined in a fixed frame ($\alpha\beta$), to obtain the estimated rotor flux $\tilde{\boldsymbol{\lambda}}_r$ and the estimated stator flux $\tilde{\boldsymbol{\lambda}}_{\boldsymbol{s}}$, also they defined in a fixed frame ($\alpha\beta$). The equations useful for obtaining the model are the magnetic equation (2.44), (2.45) and the electric stator equation (2.42). Obtaining from the equation

(2.45) $\boldsymbol{i_r}$ and replacing it in equation (2.42), the magnetic equation of stator can be rewritten as:

$$\boldsymbol{\lambda_s} = \left(1 - \frac{L_m^2}{L_r L_s}\right) L_s \boldsymbol{i_s} + \frac{L_m}{L_r} \boldsymbol{\lambda_r} \tag{2.48}$$

Using equation (2.48), the electric stator equation (2.42) can be rewritten as:

$$\boldsymbol{v_s} = R_s \boldsymbol{i_s} + \left(1 - \frac{L_m^2}{L_r L_s}\right) L_s \frac{d\boldsymbol{i_s}}{dt} + \frac{L_m}{L_r} \frac{d\boldsymbol{\lambda_r}}{dt} \tag{2.49}$$

By introducing the stator coupling factor $k_s = L_m/L_s$, the rotor leakage factor $k_r = L_m/L_r$, the total leakage factor $\sigma = (1 - k_r k_s)$ the electrical equation (2.49) becomes:

$$\boldsymbol{v_s} = R_s \boldsymbol{i_s} + \sigma L_s \frac{d\boldsymbol{i_s}}{dt} + k_r \frac{d\boldsymbol{\lambda_r}}{dt} \tag{2.50}$$

Finally, by inverting equation (2.50) it is possible to find the expression of the rotor flux reported in (2.51). Fig.2.3 shows the block diagram of the VI estimator, it is obtainable starting from equation (2.51) and passing to the Laplace domain.

$$\boldsymbol{\lambda_s} = \frac{1}{k_r} \left(\int (\boldsymbol{v_s} - R_s \boldsymbol{i_s}) dt - \sigma L_s \boldsymbol{i_s} \right) \tag{2.51}$$

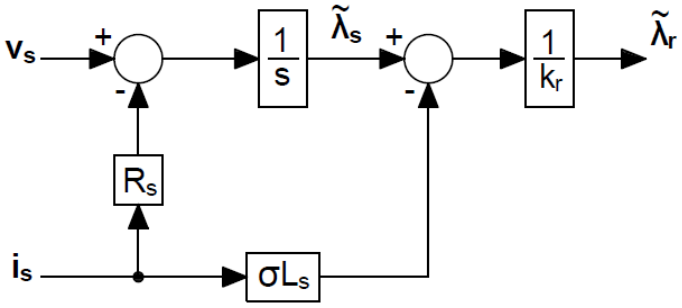

Figure 2.3: Block diagram of the flux estimator VI, which use the stator current $\boldsymbol{i_s}$ and the stator voltage $\boldsymbol{v_s}$, to obtain the estimated rotor flux $\tilde{\boldsymbol{\lambda}}_{\boldsymbol{r}}$ and the estimated stator flux $\tilde{\boldsymbol{\lambda}}_{\boldsymbol{s}}$ defined in a fixed frame ($\alpha\beta$).

The main problem of the VI is due to the presence of an integral that work in open loop. The integral in open loop systematically causes flux definition problems during low-frequency operation. Moreover the VI is sensitive to the variation of the stator resistance, but practically insensitive to the problems of magnetic saturation. Therefore, it is possible to conclude that the VI flux estimator has a good operation at high speed and is approximately independent of the load.

2.3.2 The $I\theta$ flux estimator

The $I\theta$ flux estimator ($I\theta$) uses the stator current $\boldsymbol{i_s}$ and the position of the rotor θ, respect to the fixed reference frame ($\alpha\beta$), to obtain the estimated rotor flux $\tilde{\boldsymbol{\lambda}}_{\boldsymbol{r}}$. The equations necessary to obtain this estimator are the electrical and magnetic rotor equations reported in the equation systems (2.32) and (2.33). In the case which the rotation speed ω_k of the reference frame ($\alpha_k\beta_k$) coincides with that of the rotor speed ω, the electric rotor equation can be rewritten as:

$$\mathbf{0} = R_r \boldsymbol{i_r} + \frac{d\boldsymbol{\lambda_r}}{dt} \tag{2.52}$$

On the basis of what has been said, equation (2.52) is valid only in a reference frame synchronous with the rotor. By obtaining $\boldsymbol{i_r}$ from the rotor magnetic equation and substituting it in equation (2.52), the electric rotor equation can be rewritten as:

$$M\boldsymbol{i_s} = \boldsymbol{\lambda_r} + \tau_r \frac{d\boldsymbol{\lambda_r}}{dt} \tag{2.53}$$

where $\tau_r = L_r/R_r$. Fig.2.4 shows the block diagram of the $I\theta$ estimator obtained starting from (2.53) and passing to the Laplace domain.

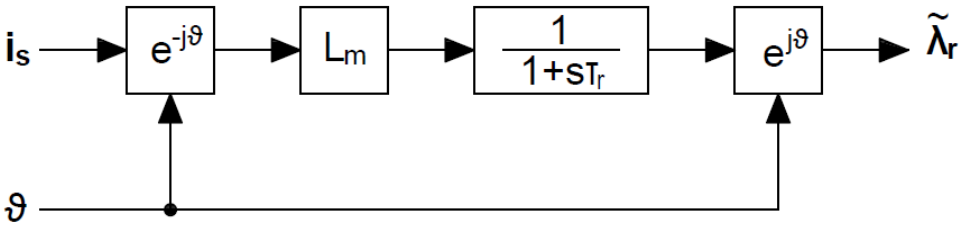

Figure 2.4: Block diagram of the $I\theta$ flux estimator, which use the stator current $\boldsymbol{i_s}$ and the position of the rotor θ, to obtain the estimated rotor flux $\tilde{\boldsymbol{\lambda}}_{\boldsymbol{r}}$ defined in a fixed frame ($\alpha\beta$).

It is useful to observe how the complex operators that appear in the block diagram shown in Fig.2.4, are the same complex operators already used to define the two-phase model of the motor. The main problems of the $I\theta$ are related to the magnetic saturation and the temperature dependence of R_r. Therefore, it is possible to conclude that with low loads and at low speeds the flux estimated using the estimator $I\theta$ is approximately correct.

2.3.3 The $VI\theta$ stator flux observer

The $VI\theta$ flux observer combines the models of the VI and $I\theta$ estimators allowing to calculate the observed stator flux $\hat{\boldsymbol{\lambda}}_{\boldsymbol{s}}$ and the observed rotor flux $\hat{\boldsymbol{\lambda}}_{\boldsymbol{r}}$.

In this thesis the $VI\theta$ was used to observe the stator flux. Fig.2.5 shows the block diagram of the observer $VI\theta$ used, from which it is possible to see how the first step is to make the difference between the two flux estimates and multiply them by G. Then, the second step is to add the difference of the estimated flux multiplied by G, at the input of the VI estimator. In this way the output In this way the rotor and stator flux estimated starting from the VI become observed flux.

It is possible to demonstrate that the observed stator flux $\hat{\boldsymbol{\lambda}}_{\boldsymbol{s}}$ is obtained from the composition of the flux estimated by the two estimators. In particular, for $\omega < G$ the estimate deriving from VI is predominant, while for $\omega > G$ the estimate deriving from $I\theta$ is predominant. So in conclusion we can say that the most accurate estimate is always used.

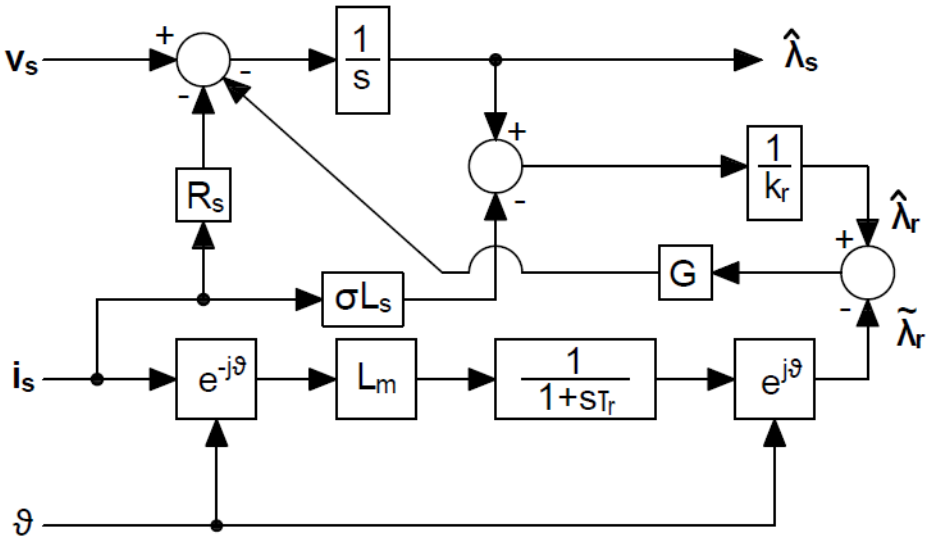

Figure 2.5: Block diagram of the $VI\theta$ flux observer, which use the stator current $\boldsymbol{i_s}$, the stator voltage $\boldsymbol{v_s}$ and the position of the rotor θ, to obtain the observed stator flux $\hat{\boldsymbol{\lambda}}_{\boldsymbol{s}}$ defined in a fixed frame ($\alpha\beta$).

In Tab.2.3 the values of the parameters used in the flux observer are shown.

2.4 Mathematical models of the 2-level Voltage Source Inverter

In this section the model of the inverter is presented, more details can be found in [23]. The inverter used in the simulations and for the experimental tests is a 2-Level Voltage Source Inverter (2L-VSI). In particular, an inverter with ideal switches was considered in the simulation. In Fig.2.6 the scheme of the inverter is shown and it is connected to a symmetrical and balanced star load without neutral, characterized by phase impedance equal to Z, this

Table 2.3: Flux observer parametrers.

Flux observer parametrers	Value
R_s	0.4095 Ω
R_r	0.4065 Ω
L_s	33.779 mH
L_r	33.779 mH
L_m	31.613 mH
G	15 rad/s

scheme is quite general and useful for understanding the operating principle. The inverter is made with six power switches, in particular it is possible to identify three legs that are: A, B and C. Each leg is made by connecting in series two power switches that work in a complementary way, to avoid the short-circuit of the DC-link. Consequently, at every instant the possible states of leg S_A, S_B, S_C can be only two. In particular, the two possible states will be indicated with $+1$ and -1, which correspond respectively to the case in which the upper or lower leg switch is closed.

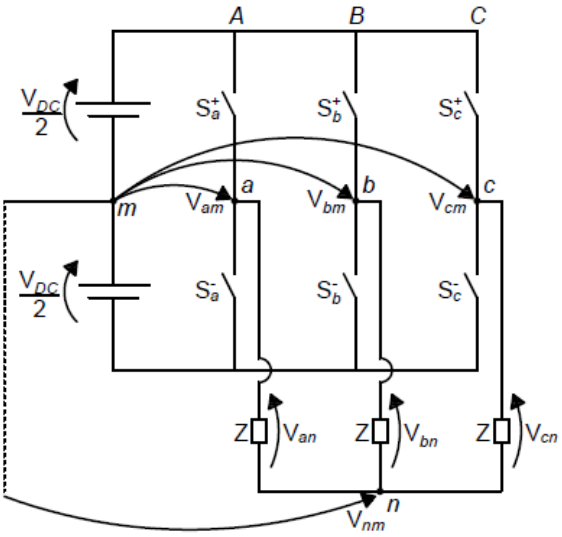

Figure 2.6: General scheme of a three-phase inverter with ideal switch connected to a symmetrical and balanced load without neutral.

Thus the voltages leg can be described as follows:

$$V_{am} = S_A \frac{V_{DC}}{2} \tag{2.54}$$

$$V_{bm} = S_B \frac{V_{DC}}{2} \tag{2.55}$$

$$V_{cm} = S_C \frac{V_{DC}}{2} \tag{2.56}$$

The load phase voltages, can be expressed as:

$$V_{an} = V_{am} - V_{nm} \tag{2.57}$$

$$V_{bn} = V_{bm} - V_{nm} \tag{2.58}$$

$$V_{cn} = V_{cm} - V_{nm} \tag{2.59}$$

In general, in industrial applications the center of the load is not accessible, so the V_{nm} voltage can not be measured, consequently the equations (2.57), (2.58) and (2.59) from the application point of view, are not useful for defining the phase voltages. But the voltage V_{nm} can however be easily written as a function of voltages leg, in fact adding a member to a member the previus equations we have that:

$$V_{an} + V_{bn} + V_{cn} = V_{am} + V_{bm} + V_{cm} - 3V_{nm} \tag{2.60}$$

From the equation (2.60), thanks to the hypothesis of symmetrical and balanced load without neutral it is possibile define V_{nm} as follows:

$$V_{an} + V_{bn} + V_{cn} = 0 \rightarrow V_{nm} = \frac{V_{am} + V_{bm} + V_{cm}}{3} \tag{2.61}$$

Using equation (2.61), it is possible to describe the phase voltages as a function of the leg voltages, with the leg voltages that can always be defined from the state of the leg. Thus the equations which allow us to express the phase voltages solely as a function of the leg voltages are:

$$V_{an} = \frac{2}{3} V_{am} - \frac{1}{3}(V_{bm} + V_{cm}) \tag{2.62}$$

$$V_{bn} = \frac{2}{3} V_{bm} - \frac{1}{3}(V_{am} + V_{cm}) \tag{2.63}$$

$$V_{cn} = \frac{2}{3} V_{cm} - \frac{1}{3}(V_{am} + V_{bm}) \tag{2.64}$$

Finally, below are the equations organized in vector form where the leg states are explicited:

$$\begin{pmatrix} V_{an} \\ V_{bn} \\ V_{cn} \end{pmatrix} = \frac{V_{DC}}{2} \begin{pmatrix} 2/3 & -1/3 & -1/3 \\ -1/3 & 2/3 & -1/3 \\ -1/3 & -1/3 & 2/3 \end{pmatrix} \begin{pmatrix} S_A \\ S_B \\ S_C \end{pmatrix} \tag{2.65}$$

As noted above, in this particular operating condition, the sum of the phase voltages is zero so we can state that the phase voltages vector belongs at any time to a plane, as a consequence they will be illustrated in a fixed referenze frame ($\alpha\beta$). Moreover, considering that the number of possible

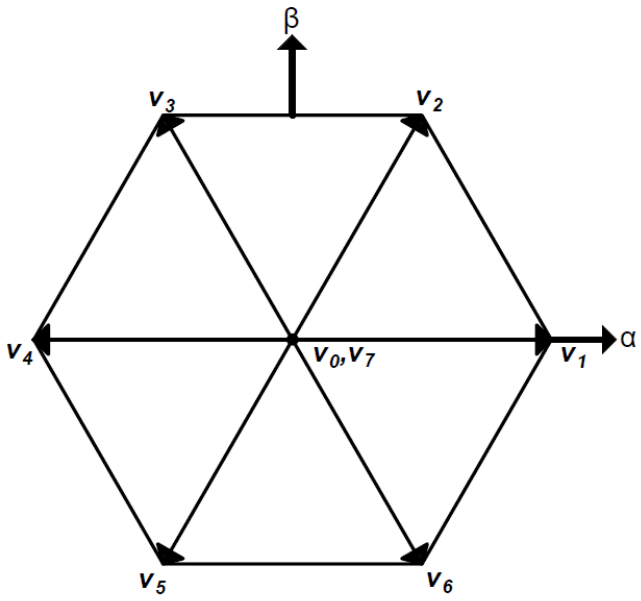

Figure 2.7: Representation of the possible voltage vectors that can be applied to the load by the three-phase inverter in the fixed reference frame (α, β).

legs states is 2 and the legs of the three-phase inverter are 3, the number of possible voltage vectors that can be applied to the load is $2^3 = 8$. Among the eight possible voltage vectors, two vectors have zero amplitude, while the other six vectors have non-zero amplitude. In particular, the two zero voltage vectors correspond to the two states in which all the upper or lower switches of the three legs are closed. Fig.2.7 shows the eight voltage vectors in the (α, β) reference frame, that are numbered from zero to seven, and it is possible to observe how the six voltage vectors different from zero made a hexagon. This representation in the literature is known as "hexagon of the output voltages of the three-phase inverter" and allows at evaluating the voltage applied to the load according to the leg states.

The components of the voltage vectors v_α and v_β in the (α, β) reference frame can be obtained using the transformation matrix B', previously used for the construction of the two-phase model of the induction machine, so we have:

$$\begin{pmatrix} v_\alpha \\ v_\beta \end{pmatrix} = \frac{2}{3} \begin{pmatrix} 1 & -1/2 & -1/2 \\ 0 & \sqrt{3}/2 & -\sqrt{3}/2 \end{pmatrix} \begin{pmatrix} V_{an} \\ V_{bn} \\ V_{cn} \end{pmatrix} \tag{2.66}$$

Tab.2.4 shows the eight possible voltage vectors, the corresponding leg states necessary to generate them, and the component value of the voltages vector on the (α, β) reference frame. It is also important to observe how the states of the three legs of inverter define the status of the inverter S.

Table 2.4: Voltage vectors that can be generated by a 2-Level Voltage Source Inverter, corresponding leg states and components in a fixed frame (α, β) for each of them.

Voltage vector	Leg States			Components of the voltage vectors	
	S_A	S_B	S_C	v_α	v_β
v_0	-1	-1	-1	0	0
v_1	+1	-1	-1	$2V_{DC}/3$	0
v_2	+1	+1	-1	$V_{DC}/3$	$\sqrt{3}V_{DC}/3$
v_3	-1	+1	-1	$-V_{DC}/3$	$\sqrt{3}V_{DC}/3$
v_4	-1	+1	+1	$-2V_{DC}/3$	0
v_5	-1	-1	+1	$-V_{DC}/3$	$-\sqrt{3}V_{DC}/3$
v_6	+1	-1	+1	$V_{DC}/3$	$-\sqrt{3}V_{DC}/3$
v_7	+1	+1	+1	0	0

Finally, we can see how the model of the inverter just obtained is already a discrete model, in fact only eight voltage vectors can be generated. This discrete nature of the three-phase inverter is the basis of all the strategies based on the FCS-MPC and therefore also of the SMPC strategy. In all this strategies the optimization problem is simplified by limiting the predictions of the behavior of the system to the eight available voltage vectors.

In the next chapter, taking advantage of the models just obtained, we will proceed to analyze and illustrate all the possible SMPC strategies based on two control stages, applied to the induction motor, in which stator flux and torque are controlled consecutively.

3
Sequential Model Predictive Control for Induction Machine

The Sequential Model Predictive Control (SMPC) strategies are a new innovation in the field of high performance electric drives. The SMPC strategies, can be considered deriving from the Finite Control Set-Model Predictive Control (FCS-MPC) of torque and flux, in fact as for FCS-MPC the discrete nature of the inverter is considered, and the controlled variables are stator flux and torque.

SMPC strategies are interesting from an application point of view, because they do not use a weighting factors. In fact, among the main problems of the FCS-MPC there is certainly the definition of the weighting factors due to the need to control variables of different nature (unit of measurement, order of magnitude) using a single cost function. The weighting factors within the cost function, allow to give more or less importance to the variables to be controlled influencing the performance of the control [5, 6]. Therefore their definition is an important step in the design of an electric drive that uses the FCS-MPC strategy. However, they are often obtained through iterative processes that are not accepted by many users [15–17].

The SMPC strategies do not use weighting factors, because perform a sequential evaluation of the cost functions associated at the torque and the stator flux, in two different stages. Therefore, we can say that with this new strategies, all the problems of definition of the weighting factors are solved. The SMPC strategies can be divided into two groups considering the order in which the cost functions are evaluated. In particular, if the flux error is evaluated in the first stage and the torque error in the second stage we will call this group of strategies SMPC-FT, where (FT) at the end of the name stand for flux and torque. In the same way, in the case in which the first stage evaluates the torque error and the second stage the flux error, we will call these SMPC-TF strategies, where this time (TF) at the end of the name stand for torque and flux.

In all the SMPC strategies analysed in this thesis the first cost function is evaluated for all the available voltage vectors, which are seven using a 2L-VSI. The first cost function, can be the torque cost function or the stator flux cost function as well also the second cost function. Then the two or at most six voltage vectors that generate the smallest torque/flux error and that

at same time have the smallest subscription are selected for the evaluation of the flux/torque error. Among the two or at most six voltage vectors available, the voltage vector that minimizes the flux/torque error and that at same time have the smallest subscription is selected.

This means that ideally there are five SMPC-TF/ SMPC-FT strategies that can be distinguished from the number of vectors used for the second minimization. To identify them, a number from two to six will be used at the end of the name.

The possible strategies SMPC-FT1, SMPC-TF1, SMPC-FT7 and SMPC-TF7 are not considered as a usable strategies. In fact for example, with the SMPC-FT1 strategy only the minimization of the flux error is carried out and the torque error is neglected, while with the SMPC-FT7 strategy exactly the opposite happens. Considering only the torque or flux error minimization does not allow the electric drive to work. The same speech is valid for the SMPC-TF1 and SMPC-TF7 strategies. Therefore, without having to analyze such strategies, it is intuitive that they are not suitable for carrying out a control of the induction machine.

One of the contributions of this thesis, is the study of all the possible SMPC strategies applied to an three-phase induction motor, when a 2-Level Voltage Source Inverter (2L-VSI) is used to supply it.

Therefore, in this chapter the strategies that allow to control the three-phase induction motor and the strategies that do not allow to control the three-phase induction motor will be identified. In particular, the main results obtained by the simulations will be presented and the reasons why not all the strategies can be used for an electric drive of an induction motor will be briefly explained.

All the analyzes carried out have been developed using the Matlab and Simulink software, moreover the aim of the results presented in this chapter is to obtain results that can be compared with what is reported in [18]. Finally, it is important to underline that all the results were obtained through the use of an induction motor model in which the phenomena of magnetic saturation, iron losses and friction coefficients were taken into consideration.

3.1 Mathematical model and figures of merit analyzed

As noted above, for the implementation of this control strategy it is necessary to consider the discrete nature of the inverter and to derive the discrete model of the induction motor. So for the sake of expository clarity, below are the equations of the induction machine expressed in a stationary frame ($\alpha\beta$) obtained in the previous chapter. Starting from these equations and using the Euler method the equations used for the prediction will be obtained.

$$\boldsymbol{v_s} = R_s \boldsymbol{i_s} + \frac{d\boldsymbol{\lambda_s}}{dt} \tag{3.1}$$

$$\mathbf{0} = R_r \boldsymbol{i_r} + \frac{d\boldsymbol{\lambda_r}}{dt} - j\omega\boldsymbol{\lambda_r} \tag{3.2}$$

$$\boldsymbol{\lambda_s} = L_s \boldsymbol{i_s} + L_m \boldsymbol{i_r} \tag{3.3}$$

$$\boldsymbol{\lambda_r} = L_m \boldsymbol{i_s} + L_r \boldsymbol{i_r} \tag{3.4}$$

$$T = \frac{3}{2} p \boldsymbol{\lambda_s} \wedge \boldsymbol{i_s} \tag{3.5}$$

$$T - T_L = J\frac{d\omega_r}{dt} \tag{3.6}$$

For the same reasons, in Fig.3.1 are shown the eight possible voltage vectors that can be generated by the 2-Level Voltage Source Inverter. In Chapter 2, it is possible to find the treatment necessary to obtain the model of the induction machine and the model of the 2-Level Voltage Source Inverter.

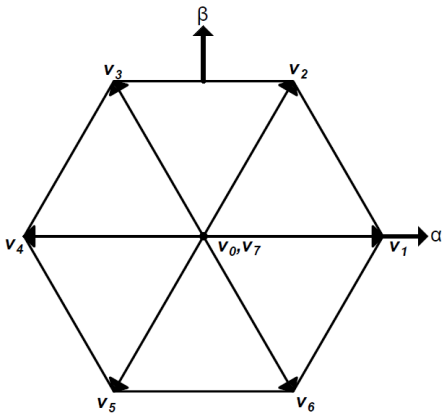

Figure 3.1: Representation in the fixed reference frame (α, β) of all the voltage vectors that can be generated by the three-phase inverter and which can be used to supply the three-phase induction motor.

For all the strategies the following figures of merit were analyzed:

- speed step response with reduced stator flux;
- response to a simultaneous load and flux step.

The first analysis was carried out with the aim of observing the ability of the strategies to control flux values that are lower than the nominal ones, considering that the control of the stator flux is a fundamental aspect when operating in a flux-weakening region. The second analysis, instead, was made to observe the functioning of the strategies when an Maximum Torque per Ampere (MTPA) strategy is used.

3.2 Equation for prediction

In this section the discrete model of the induction machine used for the implementation of all the strategies will be obtained. For all the strategies that will be illustrated a digital delay compensation has been realized. The digital delay compensation in electric drives that use MPC strategies is always important, because the calculation time are significant compared to sampling time T_s [11]. In general, the typical problems that occur when digital delay compensation is not achieved, concern the excessive ripple of the controlled variables and therefore the degradation of the performances obtainable from the electric drive. To do this, the general concept is to use the measurements and the state of the inverter at the current time k to calculate the controlled variables at the instant $k+1$. Then, note the controlled variables at the instant $k+1$, their prediction is made for the instant $k+2$ considering all the possible states of the inverter. Finally, the state of the inverter that minimizes the error between the reference and the predicted variable at the instant $k+2$ is selected. So in other words this means that the cost functions must be evalueted for the instant $k+2$.

All sequential strategies anlised use cost functions that minimize torque and stator flux errors. Consequently considering also the necessity to compensate the digital delay, it is essential to calculate the stator flux and the torque at the instant $k+2$. To do this, the variables that must be predicted at instant $k+2$ are stator flux and stator current, since the torque delivered of the machine is a function of these two variables. Moreover, since for the discretization of the equations we want to use the Euler method, it is essential to obtain, from the machine model, the equations in which $\boldsymbol{i_s}$ and $\boldsymbol{\lambda_s}$ are the only state variables that appear.

In order to obtain the equation useful for predicting of the stator current, it is first necessary to derive the rotor current $\boldsymbol{i_r}$ from the magnetic rotor equation (3.4). Then, replacing it in the magnetic stator equation (3.3), the following expression is obtained:

$$\boldsymbol{\lambda_s} = \sigma L_s \boldsymbol{i_s} + k_r \boldsymbol{\lambda_r} \tag{3.7}$$

Using equation (3.7) the electric stator equation (3.1) can be rewritten as:

$$\boldsymbol{v_s} = R_s \boldsymbol{i_s} + \sigma L_s \frac{d\boldsymbol{i_s}}{dt} + k_r \frac{d\boldsymbol{\lambda_r}}{dt} \tag{3.8}$$

To obtain an equation in which the only state variable is $\boldsymbol{i_s}$, the term $d\boldsymbol{\lambda_r}/dt$ must be removed from equation (3.8). To do this it is possible to use the electric rotor equation (3.2), and by executing the steps is possible to obtain the following expression:

$$\frac{d\boldsymbol{i_s}}{dt} = \frac{1}{\sigma L_s}\left(\boldsymbol{v_s} - \left(R_s + R_r \frac{L_s}{L_r}\right)\boldsymbol{i_s} + j\omega\sigma Ls\boldsymbol{i_s} + \frac{\boldsymbol{\lambda_s}}{\tau_r} - j\omega\boldsymbol{\lambda_s}\right) \tag{3.9}$$

The equation useful for predicting of the stator flux, is easily obtained by inverting the electric stator equation (3.1), and is as follows:

$$\frac{d\boldsymbol{\lambda_s}}{dt} = \boldsymbol{v_s} - R_s \boldsymbol{i_s} \tag{3.10}$$

In conclusion, equations (3.9) and (3.10) are the equations useful, after being discretized, to realize the stator flux and stator current prediction.

As previously noted, the $VI\theta$-flux observer ($VI\theta$) was used to implement all control strategies. From the $VI\theta$ for every instant k, exploiting the properties of the discrete integral, two information are available and they are:

- $\boldsymbol{\lambda_s}^{k+1}$ which is the predicted stator flux for the future instant $k+1$, in particular it is the output of the $VI\theta$ at the present simple k;
- $\boldsymbol{\lambda_s}^{k}$ which is the predicted stator flux for the present instant k, in particular it is the output of the $VI\theta$ at the previous simple $k-1$ kept in memory.

In fact we want to underline that the discrete integral is always in advance of the integrated signal, so it is calculated at the instant k but it indicates the information at the instant $k+1$.

The first information of the $VI\theta$ is used for the prediction of $\boldsymbol{i_s}^{k+2}$, that is the stator current at instant $k+2$ and for the prediction of $\boldsymbol{\lambda_s}^{k+2}$, that is the stator flux at the instant $k+2$. The second information is just used for the prediction of $\boldsymbol{i_s}^{k+1}$, that is the stator current at the instant $k+1$. Finally it is important to observe how at every instant k also the stator current $\boldsymbol{i_s}^{k}$ and the state of the inveter, therefore $\boldsymbol{v_s}^{k}$, are known.

For the prediction of the stator current at the instant $k+1$, the starting equation is (3.9). Discretizing equation (3.9) with the Euler method and using all the available information at the instant k it is possible to calculate $\boldsymbol{i_s}^{k+1}$. Below are shown the equations used to predict stator currents at the instant $k+1$ expressed by components.

$$\begin{cases} i_{s\alpha}^{k+1} = i_{s\alpha}^{k} + \frac{T_s}{\sigma L_s}\left(v_{s\alpha}^{k} - \left(R_s + R_r\frac{L_s}{L_r}\right) i_{s\alpha}^{k} - \omega\sigma L_s i_{s\beta}^{k} + \frac{\lambda_{s\alpha}^{k}}{\tau_r} + \omega\lambda_{s\beta}^{k}\right) \\ i_{s\beta}^{k+1} = i_{s\beta}^{k} + \frac{T_s}{\sigma L_s}\left(v_{s\beta}^{k} - \left(R_s + R_r\frac{L_s}{L_r}\right) i_{s\beta}^{k} + \omega\sigma L_s i_{s\alpha}^{k} + \frac{\lambda_{s\beta}^{k}}{\tau_r} - \omega\lambda_{s\alpha}^{k}\right) \end{cases} \tag{3.11}$$

At the same way, using $\boldsymbol{i_s}^{k+1}$ and $\boldsymbol{\lambda_s}^{k+1}$, it is possible to calculate $\boldsymbol{i_s}^{k+2}$. Below are shown the equations used to predict stator currents at the instant

$k+2$ expressed for components.

$$\begin{cases} i_{s\alpha}^{k+2} = i_{s\alpha}^{k+1} + \frac{T_s}{\sigma L_s}\left(v_{s\alpha}^{k+1} - \left(R_s + R_r\frac{L_s}{L_r}\right) i_{s\alpha}^{k+1} - \omega\sigma L_s i_{s\beta}^{k+1} + \frac{\lambda_{s\alpha}^{k+1}}{\tau_r} + \omega\lambda_{s\beta}^{k+1}\right) \\ i_{s\beta}^{k+2} = i_{s\beta}^{k+1} + \frac{T_s}{\sigma L_s}\left(v_{s\beta}^{k+1} - \left(R_s + R_r\frac{L_s}{L_r}\right) i_{s\beta}^{k+1} + \omega\sigma L_s i_{s\alpha}^{k+1} + \frac{\lambda_{s\beta}^{k+1}}{\tau_r} - \omega\lambda_{s\alpha}^{k+1}\right) \end{cases} \tag{3.12}$$

It is important to underline how in this case the voltages $v_{s\alpha}^{k+1}$ and $v_{s\beta}^{k+1}$ are the components of the $\boldsymbol{v_s}^{k+1}$, that are the possible voltage vectors usable at the instant $k+1$. For each of the voltage vectors usable at the instant $k+1$, if we want to estimate the current at the instant $k+2$ due to its application, it is necessary to use equations (3.12).

For the prediction of the stator flux at the instant $k+2$, the starting equation is (3.10). Discretizing equation (3.10) with the Euler method and using $\boldsymbol{i_s}^{k+1}$ and $\boldsymbol{\lambda_s}^{k+1}$ it is possible to calculate $\boldsymbol{\lambda_s}^{k+2}$. Below are shown the equations used to predict stator flux at the instant $k+2$ expressed by components.

$$\begin{cases} \lambda_{s\alpha}^{k+2} = \lambda_{s\alpha}^{k+1} + T_s v_{s\alpha}^{k+1} - R_s T_s i_{s\alpha}^{k+1} \\ \lambda_{s\beta}^{k+2} = \lambda_{s\beta}^{k+1} + T_s v_{s\beta}^{k+1} - R_s T_s i_{s\beta}^{k+1} \end{cases} \tag{3.13}$$

Also in this case for the voltages $v_{s\alpha}^{k+1}$ and $v_{s\beta}^{k+1}$ the same speech made previously is valid.

Known $\boldsymbol{i_s}^{k+2}$ and $\boldsymbol{\lambda_s}^{k+2}$, using the equation (3.14), it is possible to calculate also T^{k+2} that is the predicted torque at the instant $k+2$.

$$T^{k+2} = \frac{3}{2}p(\boldsymbol{\lambda_s}^{k+2} \wedge \boldsymbol{i_s}^{k+2}) = \frac{3}{2}p(\lambda_{s\alpha}^{k+2} i_{s\beta}^{k+2} - \lambda_{s\beta}^{k+2} i_{s\alpha}^{k+2}) \tag{3.14}$$

Consequently, having obtained the discrete model of the machine and having found the equations necessary to predict the value of the controlled variables, that are $\boldsymbol{\lambda_s}^{k+2}$ and T^{k+2}, it remains only to define the two cost functions.

The two cost functions, which allow to evaluate the torque and flux errors as a function of the usable voltage vectors, used in all the sequential strategies analyzed in this thesis, are:

$$\begin{cases} g_T = (T^* - T^{k+2})^2 \\ g_\lambda = (|\boldsymbol{\lambda_s}^*| - |\boldsymbol{\lambda_s}^{k+2}|)^2 \end{cases} \tag{3.15}$$

where T^* is the torque reference while $\boldsymbol{\lambda}^*$ is the stator flux reference.

Finally, we want to observe how to perform the evaluation of the cost function g_T in the general case. To do this we consider that the number

of voltage usable at the instant $k+1$ is N. To identify the generic voltage vectors, the subscript n is added (with $n \in N$) so they will be called $\boldsymbol{v_s}_n^{k+1}$. At the same way, to all the quantities estimated using $\boldsymbol{v_s}_n^{k+1}$, the subscript n is added. At the instant k known $\boldsymbol{i_s}^k$ and $\boldsymbol{\lambda_s}^k$ it is possible to estimate $\boldsymbol{i_s}^{k+1}$ using equations (3.11). From the estimates of $\boldsymbol{\lambda_s}^{k+1}$, $\boldsymbol{i_s}^{k+1}$ and known the N usable $\boldsymbol{v_s}_n^{k+1}$, it is possible to estimate the $\boldsymbol{i_s}_n^{k+2}$ resulting from the application of each of the $\boldsymbol{v_s}_n^{k+1}$, using equations (3.12). In particular the number of the $\boldsymbol{i_s}_n^{k+2}$ estimated is N. From the estimates of $\boldsymbol{\lambda_s}^{k+1}$, $\boldsymbol{i_s}^{k+1}$ and known the N usable $\boldsymbol{v_s}_n^{k+1}$ it is possible to estimate the $\boldsymbol{\lambda_s}_n^{k+2}$ resulting from the application of each of the $\boldsymbol{v_s}_n^{k+1}$, using equations (3.13). Also in this case the number of the $\boldsymbol{\lambda_s}_n^{k+2}$ estimated is N. At the end of this procedure, it will then be possible to calculate N differents torque, using the following expression:

$$T_n^{k+2} = \frac{3}{2} p(\boldsymbol{\lambda_s}_n^{k+2} \wedge \boldsymbol{i_s}_n^{k+2}) \tag{3.16}$$

Each of the one N calculated torques is used to evaluate the g_T, and finally on the basis of the torque error it is possible to proceed with the selection of the voltage vectors. For all the N calculated torque, the cost function g_T will be evaluated. The same procedure is valid for the evaluation of the g_λ cost function.

3.3 SMPC-TF strategies

The SMPC-TF strategies perform a sequential evaluation of the cost functions and are based on two-stages, in which the single cost function is evaluated. In particular in these stretegies the first stage controls the torque and the second stage controls the flux. Fig.3.2 shows the block diagram of the SMPC-TF strategies applied to the induction machine.

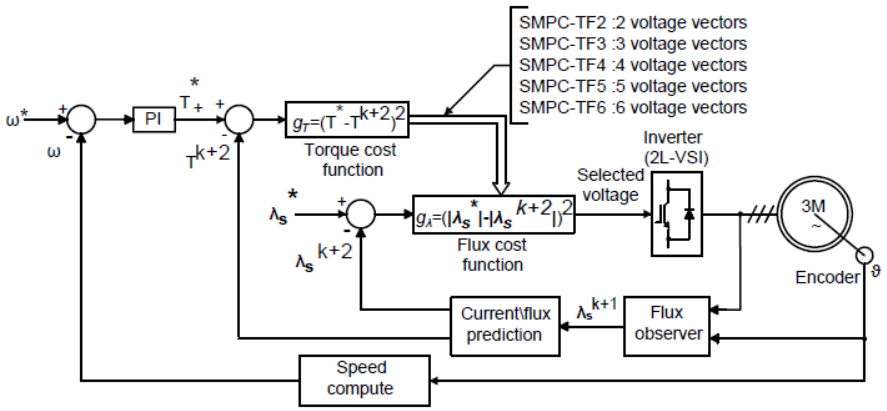

Figure 3.2: Block diagram of SMPC-TF strategies.

During its operation, the SMPC-TF control strategies start by calculating the speed error between the reference speed ω^* and the actual speed of the motor ω. The speed error is introduced in a Proportional-Integral (PI) controller, from which the reference torque T^* is obtained. Calculated T^*, is possible to proceed with the evaluation of the cost function g_T by calculating T^{k+2} for all seven voltage vectors available from 2L-VSI. It should be noted that for the evaluation of g_T, T^* is assumed constant between the instant k and $k+2$, this assumption can be considered valid since generally the mechanical time constants are greater than the electrical ones. Then the two or at most six voltage vectors that generate the smallest g_T value and that at same time have the smallest subscription are used for the evaluation of g_λ. With g_λ that can be evaluated, known the reference flux $\boldsymbol{\lambda_s}^*$ and estimated $\boldsymbol{\lambda_s}^{k+2}$ for the two or at most six voltage vectors deriving from the minimization of g_T. Finally, between the available two or at most six voltage vectors, the voltage vector that minimizes g_λ and that at same time have the smallest subscription is selected as global optimal and applied through the inverter.

Since the strategies applied to an induction machine, it is essential to provide an initial fluxing phase of the machine. During the fluxing phase to limit the initial currents, the selected optimal voltage vector is applied only if the imposed current limit ($|\boldsymbol{i}_{lim}| = 35A$) is not exceeded. In the case in which the application of the voltage vector would cause a current higher than $|\boldsymbol{i}_{lim}|$, the $\boldsymbol{v_0}$ voltage vector is applied.

As previously mentioned, for the evaluation of the strategies we analyzed:

- speed step response with reduced stator flux;
- response to a simultaneous load and flux step.

In particular, from $0s$ to $0.2s$ the machine is fluxed to $0.6Vs$, which is 75% of the nominal flux. At $0.2s$ a speed step is required, by imposing $\omega^* = 100rad/s$. At $0.5s$, a stepped increment of the stator flux of $0.2Vs$ and a load step equal to $40Nm$ are required.

The main control parameters used to test the SMPC-TF strategies are shown in Tab.3.1.

Table 3.1: The main control parametres.

Sample Time T_s	$1{\cdot}10^{-4}$ (s)
$DC{-}link\ voltage : V_{DC}$	$510\ V$
$Bandwidth\ speed\ regulator : \omega_b$	$2\pi \cdot 50$ (rad/s)
$Proportional\ gain\ of\ the\ speed\ regulator : k_p$	$\omega_b \cdot J$
$Integral\ gain\ of\ the\ speed\ regulator : k_i$	$\omega_b^2 \cdot J$

3.3.1 Results obtained from the simulations of the SMPC-TF2 and SMPC-TF3 startegies

The strategies SMPC-TF2 and SMPC-TF3 differ only by the number of vectors used for the evaluation of the cost function related to the stator flux g_λ. Practically, in SMPC-TF2 the vectors used for the evaluation of the g_λ are the two vectors that generate the smallest torque error g_T and that at same time have the smallest subscription. While, in SMPC-TF3 the vectors used for the evaluation of the g_λ are the three vectors that generate the smallest g_T and that at same time have the smallest subscription.

The two strategies, presented in this section, are also the only two strategies belonging to group SMPC-TF, with under the conditions indicated above it is possible to control the machine. For the two strategies, the analyzes conducted have returned very similar results, so below are reported only the results obtained with the SMPC-TF2 strategy.

Fig.3.3 shows the results obtained from the simulation of SMPC-TF2. It is possible to observe how with this strategy the speed reference is followed without any evident problem.

It is also interesting to observe how thanks to the introduction of the current limitation, described above, the average stator current value never exceeds $35A$. In particular, the current limitation intervenes in the first phase of the fluxing, before that the stator flux reaches the reference stator flux $|\boldsymbol{\lambda_s}^*| = 0.6Vs$. Moreover, it is possibile to see that at $0.2s$, also the rotor flux reaches its state steady value, which is approximately equal to that of the stator (low impact of the leakage inductances). Furthermore, it is also possible to observe how the rotor flux increases more slowly than the stator flux. In fact, it is necessary to consider the rotor time constant and it is precisely for this reason, that it is essential to provide a fluxing phase in the electric drives that use the induction motor.

Observing from Fig.3.3 the stator flux and the torque, it is possible to notice how despite the sequential evaluation of the cost functions it is possible to obtain the decoupling between stator flux and torque. In fact, at $0.2s$ when the load step is required, the stator flux module is kept under control at $0.6Vs$.

The same can be observed at the end of the transient speed. Finally, at $0.5s$ a contemporany step of load and stator flux are required, and it is possible to observe how the control strategy can satisfy this request without lost the torque or flux control.

In any case it is important to underline how such a decoupling between stator flux and torque is always guaranteed when working with nominal stator flux values. In case $|\boldsymbol{\lambda_s}^*| < 0.6Vs$ such decoupling is not guaranteed in all operating conditions. This happens because the choice of vectors deriving from torque minimization are not suitable for controlling the flux. So in practice it is possible to state that flux control is only guaranteed in

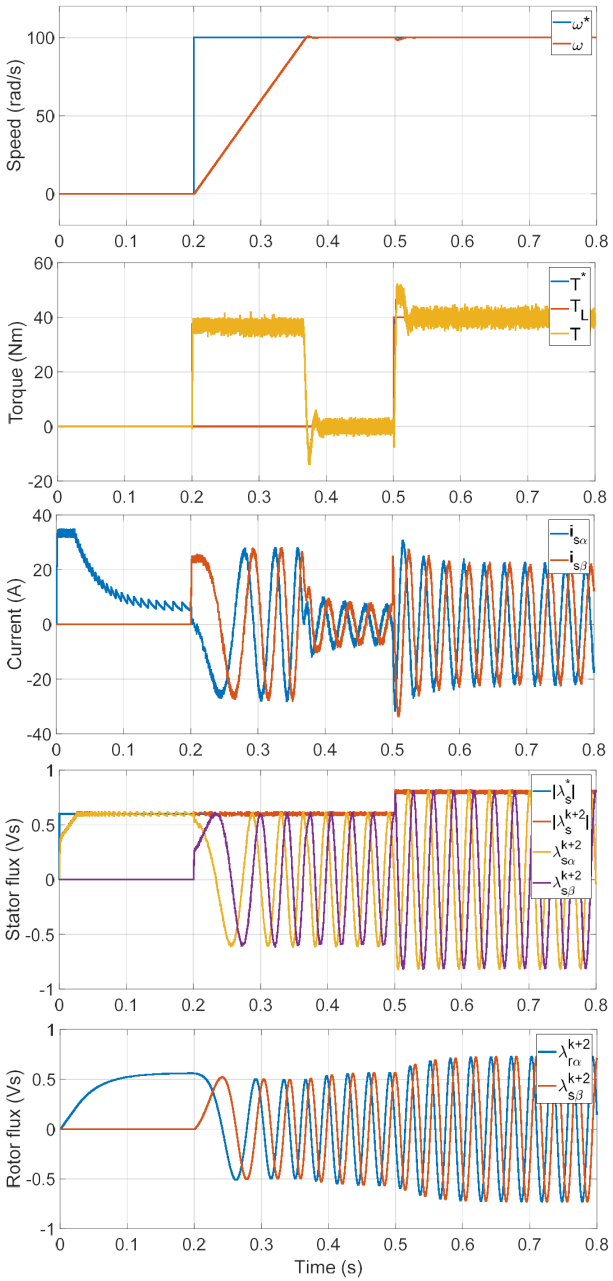

Figure 3.3: Response to the speed step and the simultaneous flux and torque step using the SMPC-TF2 strategy. From top to bottom: reference, and motor speed (rad/s); reference, load and motor torque (N·m); measured component in ($\alpha\beta$) axis of the current (A); magnitude reference, magnitude predicted and predicted components in ($\alpha\beta$) axis of the stator flux (V·s), predicted components in ($\alpha\beta$) axis of the rotor flux (V·s).

certain operating conditions and that large flux-weakening regions are not permitted.

Finally, it is also possible to observe how the stator currents, expecially when $T^* = 0$, are particularly distorted. The main causes of this distortion are due to the variable switching frequency and also to the absence of amplitude modulation of the applied voltage vectors.

Following are brief explanations of why with the SMPC-TF2 and SMPC-TF3 strategies it is possible to correctly control the induction motor.

Analysis of the SMPC-TF2 strategy

For the SMPC-TF2 strategy, the voltage vectors selected, to evaluate g_λ, are the two voltage vectors that have the lowest subscript and at the same time generate the smallest torque error g_T. From $0s$ to $0.2s$ the torque reference T^* is zero, in fact the speed reference ω^* is zero. At the first control step, all seven available voltage vectors generate the same value of g_T. Consequently, the vectors selected by the first stage for evaluating g_λ are $\boldsymbol{v_0}$ and $\boldsymbol{v_1}$, in fact they are the two voltage vectors with a lower subscript. The vector that minimizes g_λ is $\boldsymbol{v_1}$ because it is able to start the fluxing of the machine, consequently $\boldsymbol{v_1}$ is the selected vector and applied through the inverter, at the machine, to the first control step. As can be seen from Fig.3.3, thanks to the application of vector $\boldsymbol{v_1}$ the stator flux in the α-axis starts to increase.

From the second control step up to $0.2s$, the two voltage vectors selected from the first stage will continue to be $\boldsymbol{v_0}$ and $\boldsymbol{v_1}$, but the reason for which they are selected changes. In fact, $\boldsymbol{v_0}$ and $\boldsymbol{v_1}$ are the first two voltage vectors that if applied to the machine, even if the flux in the α-axis is different from zero, allow $T^{k+2} = 0$. In other word with this two voltage vectors is possible to have $g_T = 0$. So the only two vectors that can be used in the second stage, for the evaluation of g_λ are $\boldsymbol{v_0}$ and $\boldsymbol{v_1}$. The voltage vector $\boldsymbol{v_0}$ is selected when $|\boldsymbol{\lambda_s}^{k+2}| > |\boldsymbol{\lambda_s}^*|$ or if the current limitation is exceeded, while the voltage vector $\boldsymbol{v_1}$ is selected when $|\boldsymbol{\lambda_s}^{k+2}| < |\boldsymbol{\lambda_s}^*|$.

At $0.2s$ as soon as $w^* \neq 0$ and then $T^* \neq 0$, the two vectors deriving from the evaluation of g_T are instead $\boldsymbol{v_2}$ and $\boldsymbol{v_3}$. In fact, the vectors $\boldsymbol{v_2}$ and $\boldsymbol{v_3}$ are the only two voltage vectors that if applied to the machine allow to have $T \neq 0$ and positive, so they are the only two voltage vectors that allow to reduce the value of g_T. The voltage vector selected by the second stage, to the first control step after $0.2s$, is $\boldsymbol{v_3}$ because it is the one which allows to reduce the error of flux.

The principle with which the vectors are selected remains the same even when the machine is rotating. The only difference is the presence of current and stator flux in both the axes ($\alpha\beta$) of the machine, but in any case it is possible to justify the choices made by the control strategy in the same way.

Finally, as shown in Fig.3.3, using for the evaluation of g_λ, only the

two voltage vectors that generate the smallest g_T, it is possible to control simultaneously the stator flux and the torque of the induction motor.

Analysis of the SMPC-TF3 strategy

For the SMPC-TF3 strategy, the voltage vectors selected to evaluate g_λ, are the three voltage vectors that have the lowest subscript and at the same time generate the smallest torque error g_T. Also in this case from $0s$ up to $0.2s$ $T^* = 0$, and at the first control step all seven available voltage vectors generate the same value of g_T. In particular the vectors selected at the first control step, from the first stage are $\boldsymbol{v_0}$, $\boldsymbol{v_1}$ and $\boldsymbol{v_2}$ in fact they are the three vectors with lower index. From the second stage the vector selected and applied to the machine is $\boldsymbol{v_1}$, as in the previous case. In fact, $\boldsymbol{v_1}$ is able to flux the machine and therefore reduce the flux error, while $\boldsymbol{v_2}$ is not used because it has a higher subscript. In this way, thanks to the application of vector $\boldsymbol{v_1}$ the flux in the α-axis starts to increase.

From the second control step up to $0.2s$, the vectors selected by the minimization of g_T are $\boldsymbol{v_0}$, $\boldsymbol{v_1}$ and $\boldsymbol{v_4}$. In fact $\boldsymbol{v_0}$, $\boldsymbol{v_1}$ and $\boldsymbol{v_4}$ are the only three vectors that if applied to the machine even if the flux in the α-axis is different from zero allow to have $T^{k+2} = 0$. In other words they are the only three voltage vectors that allow to have $g_T = 0$. So the only three vectors that can be used in the second stage, for the evaluation of g_λ are $\boldsymbol{v_0}$, $\boldsymbol{v_1}$ and $\boldsymbol{v_4}$.

Between these three voltage vectors, $\boldsymbol{v_0}$ and $\boldsymbol{v_1}$ are used in the second stage during fluxing machine. In particular $\boldsymbol{v_1}$ is used when $|\boldsymbol{\lambda_s}^{k+2}| < |\boldsymbol{\lambda_s}^*|$, while $\boldsymbol{v_0}$ is used when $|\boldsymbol{\lambda_s}^{k+2}| > |\boldsymbol{\lambda_s}^*|$ or if the current limitation is exceeded. The $\boldsymbol{v_4}$ vector may be useful in the moments when $|\boldsymbol{\lambda_s}^{k+2}| > |\boldsymbol{\lambda_s}^*|$, is not used because it causes an error greater than that produced by $\boldsymbol{v_0}$. In fact, usining $\boldsymbol{v_4}$ instead of $\boldsymbol{v_0}$ when $|\boldsymbol{\lambda_s}^{k+2}| > |\boldsymbol{\lambda_s}^*|$ would increase the magnitude of the stator flux ripple.

Also in this case, the principle with which the vectors are selected when the machine starts to rotate remains similar to the one just illustrated.

Finally it is possible to conclude that using for the evaluation of g_λ, only the three voltage vectors that generate the smallest g_T, it is possible to control simultaneously the stator flux and the torque of the induction motor.

3.3.2 Results obtained from the simulations of SMPC-TF4, SMPC-TF5 and SMPC-TF6 strategies

The SMPC-TF4, SMPC-$TF5$ and SMPC-TF6 strategies differ only by the number of vectors used for the evaluation of the stator flux error g_λ. In particular, the number of vectors used for the minimization of the g_λ is the number reported at the end of the name.

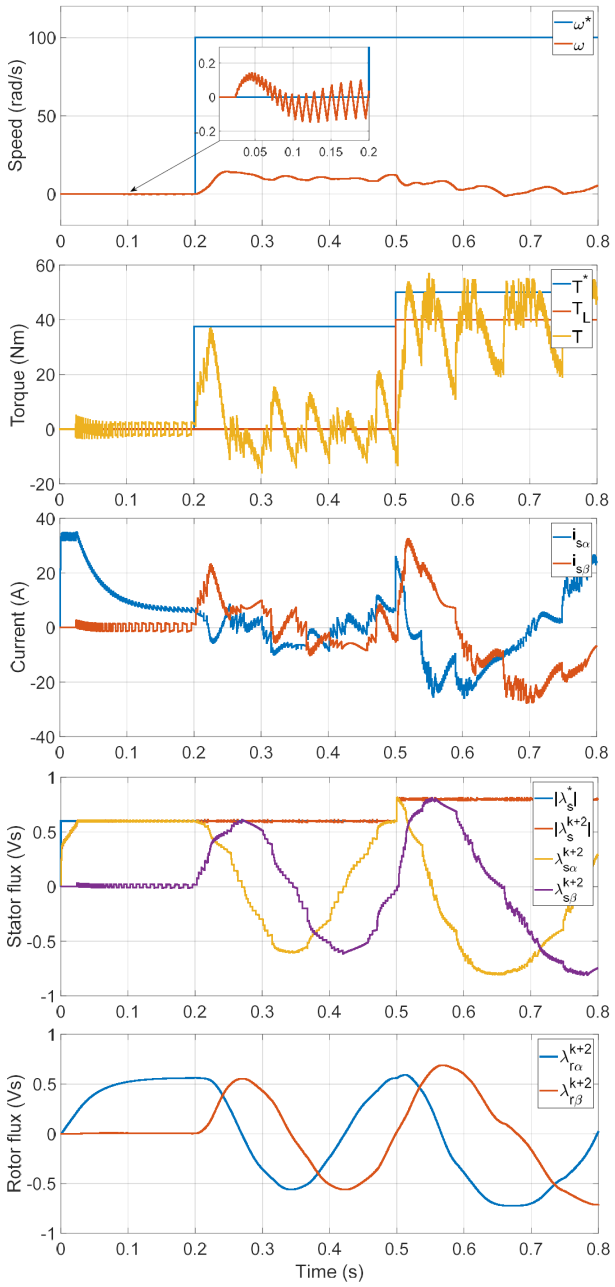

Figure 3.4: Response to the speed step and the simultaneous flux and torque step using the SMPC-TF4 strategy. From top to bottom: reference, and motor speed (rad/s); reference, load and motor torque (N·m); measured component in ($\alpha\beta$) axis of the current (A); magnitude reference, magnitude predicted and predicted components in ($\alpha\beta$) axis of the stator flux (V·s), predicted components in ($\alpha\beta$) axis of the rotor flux (V·s).

The three strategies presented in this section do not allow the control of the machine in any operating condition. As an example, in Fig.3.4 the results obtained by using the SMPC-TF4 strategy are shown.

From Fig.3.4 it is possible to observe how, also with this strategy, during the fluxing of the machine the current limitation allows not to exceed the limit of current imposed at $35A$. With SMPC-TF4 is possible to flux the machine and in fact the stator flux reaches the reference $|\boldsymbol{\lambda_s}^*| = 0.6Vs$. As a result, the rotor flux also increases and reaches the steady-state value at $0.2s$.

But the first problem observable from Fig.3.4, is the presence of torque and speed noise during the fluxing of the machine, despite $T^* = 0$ and $\omega^* = 0$. Therefore we understand that the vectors selected by the minimization of g_λ are not suitable for the control of the machine during the fluxing phase. Moreover can also be observed as at $0.2s$, when a speed/torque step are requered, the magnitude of the stator flux is controlled, but the currents are highly distorted and moreover with this strategy it is not possible to follow the torque/speed references. The same problems just illustrated, occur with the SMPC-TF5 and SMPC-TF6 strategies.

Analysis of the SMPC-TF4, SMPC-TF5 and SMPC-TF6 strategies

The analysis below refers to the SMPC-TF4 strategy, but in any case it can be easily extended to the strategies SMPC-TF5 and SMPC-TF6. For the SMPC-TF4 strategy, the voltage vectors selected to evaluate g_λ, are the four voltage vectors that have the lowest subscript and at the same time generate the smallest torque error g_T. Also in this case from $0s$ up to $0.2s$ $T^* = 0$, and at the first control step all seven available voltage vectors generate the same value of g_T. The vectors selected at the first control step, from the first stage are $\boldsymbol{v_0}$, $\boldsymbol{v_1}$, $\boldsymbol{v_2}$ and $\boldsymbol{v_3}$ in fact they are the four vectors with lower index. From the second stage the vector selected and applied to the machine is $\boldsymbol{v_1}$, as in the previous cases. In fact, $\boldsymbol{v_1}$ is able to flux the machine and therefore reduce the flux error, while $\boldsymbol{v_2}$ and $\boldsymbol{v_3}$ are not used because they have a higher subscript. As can be seen in Fig.3.4, thanks to the application of the vector $\boldsymbol{v_1}$ the stator flux in the alpha-axis starts to increase. Therefore, from the second control step the three voltage vectors that if used to supply the machine allow to have $T^{k+2} = 0$ are $\boldsymbol{v_0}$, $\boldsymbol{v_1}$ and $\boldsymbol{v_4}$. In other words, $\boldsymbol{v_0}$, $\boldsymbol{v_1}$ and $\boldsymbol{v_4}$ are the only three vectors that allow to have $g_T = 0$. The fourth vector in any case during the fluxing of the machine if used to sapplay the machine causes $g_T \neq 0$.

From the second control stage, i.e. from the minimization of g_λ as long as $|\boldsymbol{\lambda_s}^{k+2}| < |\boldsymbol{\lambda_s}^*|$ the vector selected and applied to the machine is $\boldsymbol{v_1}$ if the current limit is not exceeded, so it is possible to have $g_T = 0$. But, as soon as the stator flux reaches the reference stator flux $|\boldsymbol{\lambda_s}^*| = 0.6Vs$, the

fourth vector resulting from the minimization of g_T is $\boldsymbol{v_2}$. The vector $\boldsymbol{v_2}$, at that moment is also the vector that allows to obtain the smallest value of g_λ for which it is applied to the machine. Using the $\boldsymbol{v_2}$ vector to supplay the machine, causes the increase of the current in the β-axis and therefore the presence of torque and speed noise during the fluxing phase as can be seen from Fig.3.4. In fact, by using $\boldsymbol{v_2}$, the current $i_{s\beta}$ becomes different zero and in addition having $\lambda_{s\alpha} \neq 0$ the machine starts delivering torque. But the main problem is that at $0.2s$ as soon as $\omega^* \neq 0$ and then $T^* \neq 0$, the fourth vector which does not allow to control the torque, is often selected by the minimization of the stator flux error. From Fig.3.4 it is possible to observe how with this strategy the stator flux can be controlled, but the torque control is lost. As a result, this strategy is not able to control the machine, and we also understand that the maximum number of voltage vectors usable for minimizing g_λ, is three. In fact, if the number of voltage vector used is greater than three, the flux control is guaranteed, but not torque control therefore the strategies SMPC-F4, SMPC-TF5 and SMPC-TF6 are not usable.

3.4 SMPC-FT strategies

The SMPC-FT strategies perform a sequential evaluation of the cost functions and are based on two-stages, in which the single cost function is evaluated. In particular in these stretegies the first stage controls the stator flux and the second stage controls the torque. Fig.3.5 shows the block diagram of the SMPC-FT strategies applied to an induction machine.

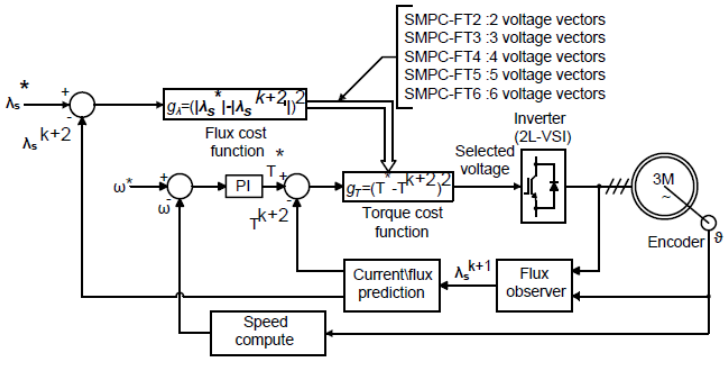

Figure 3.5: Block diagram of SMPC-FT strategies.

During its operation, the SMPC-FT control strategies start from the evaluation of g_λ. In particular, g_λ is evaluated by making the difference between the refence stator flux $|\boldsymbol{\lambda_s}^*|$ and the estimated stator flux $|\boldsymbol{\lambda_s}^{k+2}|$ for all seven voltage vectors available from 2L-VSI. Then the two or at most six voltage vectors that generate the smallest value of g_λ and that

at same time have the smallest subscription are used to calculate T^{k+2}. Finally known the speed error, using the Proportiona-Integral (PI) the T^* is calculated, and consequently it is possible to proceed with the evaluation of the g_T for all the available voltage vectors. Between the available two or at most six voltage vectors, the voltage vector that minimizes g_T and that at same time have the smallest subscription is selected as global optimal and applied through the inverter.

Also in this case using the same hypothesis made for the SMPC-TF strategies, T^* is assumed constant between the instant k and $k+2$.

Since the strategies applied to an induction machine, it is essential to provide an initial fluxing phase of the machine. During the fluxing phase to limit the initial currents, the selected optimal voltage vector is applied only if the imposed current limit ($|\boldsymbol{i}_{lim}| = 35A$) is not exceeded. In the case in which the application of the voltage vector would cause a current higher than $|\boldsymbol{i}_{lim}|$, the null voltage vector is applied. As previously mentioned, for the evaluation of the strategies we analyzed:

- speed step response with reduced stator flux;
- response to a simultaneous load and flux step.

In particular, from $0s$ to $0.2s$ the machine is fluxed to $0.6Vs$, which is 75% of the nominal flux. At $0.2s$ a speed step is required, by imposing $\omega^* = 100rad/s$. At $0.5s$, a stepped increment of the stator flux of $0.2Vs$ and a load step equal to $40Nm$ are required.

Finally, as regards the main control parameters, they are the same as those used to analyze the SMPC-TF strategies, so it is possible to refer to Tab.3.1.

3.4.1 Results obtained from the simulations SMPC-FT2 strategy

In the SMPC-FT2 the number of voltage vectors used for the evaluation of the cost function related to the torque g_T are two. In particular are the two voltage vector that generate the smallest flux error and that at same thime hav the smallest subscription.

From Fig.3.6 it is possible to observe how, also with this strategy, during the fluxing of the machine the current limitation allows not to exceed the limit of current imposed at $35A$.

Moreover with SMPC-FT2 is possible to flux the machine and in fact the stator flux reaches the reference $|\boldsymbol{\lambda_s}^*| = 0.6Vs$ and as a result, the rotor flux also increases and reaches the steady-state value at $0.2s$. But already during the fluxing phase the first problems are observed, in fact, despite $T^* = 0$ and $\omega* = 0$, torque and speed noise are observed. Therefore it is possible to state that the vectors selected by the second control stage are not suitable to respect the torque reference.

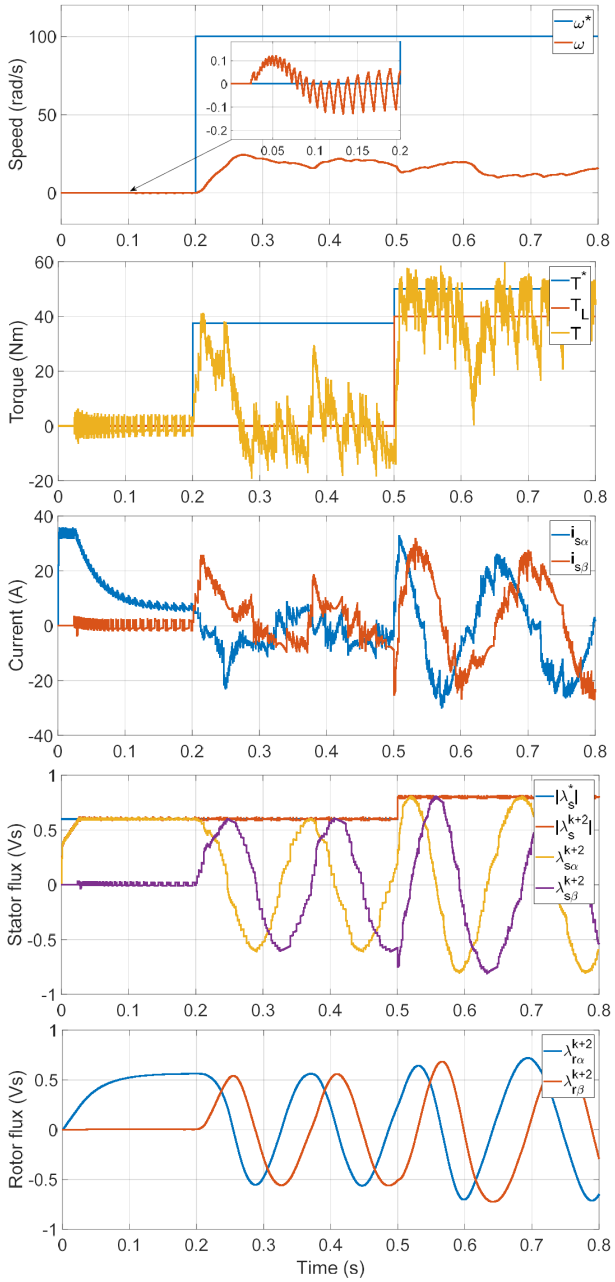

Figure 3.6: Response to the speed step and the simultaneous flux and torque step using the SMPC-FT2 strategy. From top to bottom: reference, and motor speed (rad/s);reference, load and motor torque (N·m); measured component in ($\alpha\beta$) axis of the current (A); magnitude reference, magnitude predicted and predicted components in ($\alpha\beta$) axis of the stator flux (V·s), predicted components in ($\alpha\beta$) axis of the rotor flux (V·s).

From Fig.3.6 it is also possible to observe how this strategy is not able to follow the torque and speed reference. Moreover, a high ripple of torque and current is observed, this allow us to understand how the vectors selected by the second control stage are not absolutely suitable for the minimization of torque error.

Finally, it is possible to note how with this strategy the flux reference is followed, but not the torque reference, so we can conclude that this strategy is not suitable for the control of the induction motor.

Analysis of the SMPC-FT2 and SMPC-FT6 strategies

For the SMPC-FT2 strategy, the voltage vectors selected to evaluate g_T, are the two voltage vectors that have the lowest subscript and at the same time generate the smallest flux error. Also in this case from $0s$ to $0.2s$ $T^* = 0$, and at the first control step all seven available voltage vectors generate the same value of g_λ.

The vectors selected at the first control step, from the first stage are $\boldsymbol{v_1}$ and $\boldsymbol{v_2}$ in fact they are the two vectors with lower indext able to flux the induction motor. From the second stage the vector selected and applied to the machine is $\boldsymbol{v_1}$. The vector $\boldsymbol{v_1}$ is selected only because with subscript inferior to $\boldsymbol{v_2}$, in fact with both the torque predicted $T^{k+2} = 0$ being $\boldsymbol{i_s} = 0$ at the first step control. As can be seen from Fig.3.6 thanks to the application of the vector $\boldsymbol{v_1}$ the stator flux in the alpha-axis starts to increase.

From the second control step until when $|\boldsymbol{\lambda_s}^{k+2}|$ reaches the reference $|\boldsymbol{\lambda_s}^*|$, the two voltage vectors selected by the first control stage are $\boldsymbol{v_1}$ and $\boldsymbol{v_2}$. In particular, only $\boldsymbol{v_1}$ is applied to the machine whenever the predicted current does not exceed $\boldsymbol{i_{lim}}$, in fact $\boldsymbol{v_1}$ is the only vector between the two available with which it is possible to respect the torque reference $T^* = 0$.

As soon as the stator flux reaches the reference, the two vectors selected by the first control stage are $\boldsymbol{v_2}$ and $\boldsymbol{v_6}$. The problem is that both these vectors if applied to the machine cause $T \neq 0$ since $\lambda_{s\alpha} \neq 0$. In other words they are not able to respect the torque reference during the fluxing phase. In particular, from the second control stage the voltage vector $\boldsymbol{v_2}$ is selected and used to supply the induction motor, starting the torque and speed noise as can be seen from Fig.3.3. The vector $\boldsymbol{v_2}$ is chosen instead of the $\boldsymbol{v_2}$ only because it has a lower subscript.

At $0.2s$ with $w^* \neq 0$ and then $T^* \neq 0$, in the istant in wich $|\boldsymbol{\lambda_s}^{k+2}| > |\boldsymbol{\lambda_s}^*|$ the vectors selected by the first control stage are $\boldsymbol{v_0}$ and if possible a voltage vector that is in opposition phase to the stator flux vector. Therefore it means that for several control instants, the voltage vectors available for the second control stage do not allow any torque regulation, this makes it impossible to follow the speed/torque reference. Therefore, in order to avoid these situations, the number of vectors deriving from the first minimization must be greater than two.

Instead with the SMPC-FT6 strategy is possible to follow the torque reference and no problem occurs during the fluxing phase. The main problem of this strategy is related to the high number of voltage vectors that can be used for the minimization of torque error. In fact, due to the high number of voltage vectors that can be used for the minimization of g_T, the amplitude of the flux has a high ripple which is also the cause of excessive torque ripple.

3.4.2 Results obtained from the simulations SMPC-FT3, SMPC-FT4 and SMPC-FT5 strategies

The strategies SMPC-FT3, SMPC-FT4 and SMPC-FT5 differ only by the number of vectors used for the evaluation of the cost function related to the torque g_T. In particular the number of the voltage vector used for the minimization of g_T is the number reported at the edn of name. The three strategies, presented in this section, are also the only two strategies belonging to group SMPC-FT, with under the conditions indicated above it is possible to control the machine. For the three strategies, the analyzes conducted have returned very similar results, so we have decided to report only the results for the SMPC-FT3 strategy. Fig.3.7 shows the results obtained from the simulation of SMPC-FT3. It is possible to observe how there are no particular differences respect to the strategies SMPC-TF2 and SMPC-TF3. All the considerations made previously for cases SMPC-TF2 and SMPC-TF3 can be considered valid also in this case.

Analysis of the SMPC-FT3 and SMPC-FT4 strategies

For the SMPC-FT3 strategy, the voltage vectors selected to evaluate g_T, are the three voltage vectors that have the lowest subscript and at the same time generate the smallest flux error. Also in this case from $0s$ up to $0.2s$ $T^* = 0$, and at the first control step all seven available voltage vectors generate the same value of g_λ. The vectors selected at the first control step, from the first stage are $\boldsymbol{v_1}$, $\boldsymbol{v_2}$ and $\boldsymbol{v_3}$ in fact they are the three vectors with lower subscription able to flux the induction motor. From the second stage the vector selected and applied to the machine is $\boldsymbol{v_1}$. The vector $\boldsymbol{v_1}$ is selected only because with subscript inferior to $\boldsymbol{v_2}$ and $\boldsymbol{v_3}$, in fact in any case with all three voltage vectors we have $T^{k+2} = 0$ being $\boldsymbol{i_s} = 0$ at the first step control.

Thanks to the application of the vector $\boldsymbol{v_1}$ the stator flux in the α-axis starts to increase. From $0s$ to $0.2s$ during the fluxing phase, at each instant control between the three voltage vectors selected at the first control stage the $\boldsymbol{v_0}$ or $\boldsymbol{v_1}$ vectors are always present. In this way, at each control instant there is the possibility to select a voltage vector from the second control stage that returns $T^{k+2} = 0$. Therefore during the fluxing phase there are no problems of torque/speed noise.

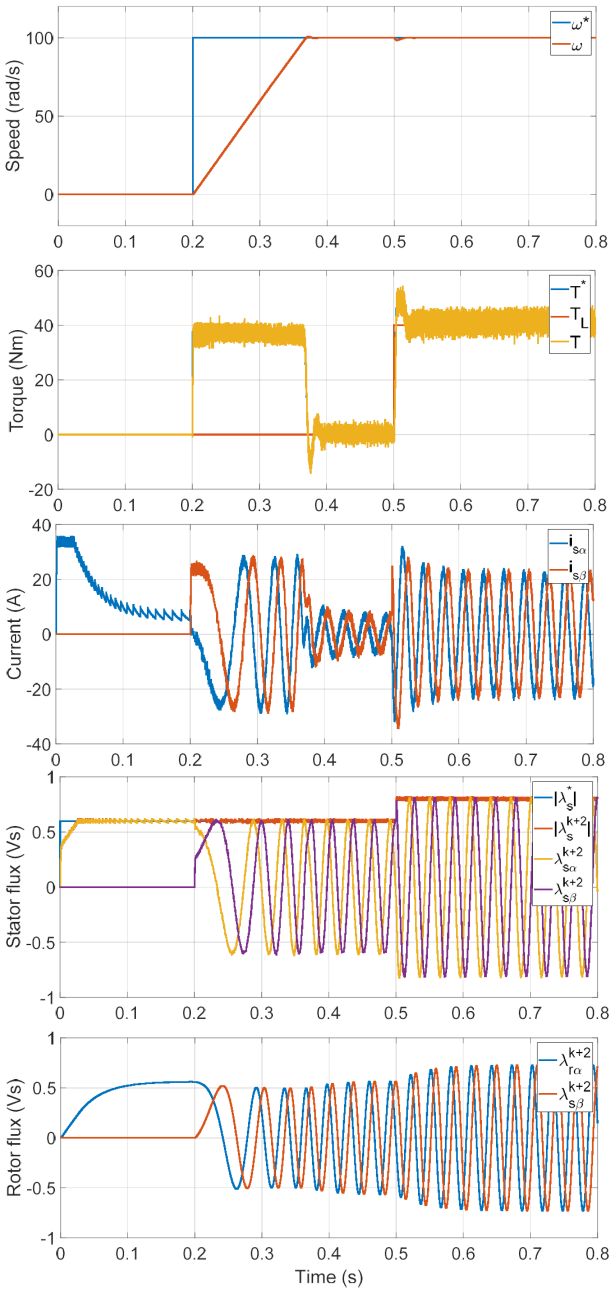

Figure 3.7: Response to the speed step and the simultaneous flux and torque step using the SMPC-FT3 strategy. From top to bottom: reference, and motor speed (rad/s);reference, load and motor torque (N·m); measured component in ($\alpha\beta$) axis of the current (A); magnitude reference, magnitude predicted and predicted components in ($\alpha\beta$) axis of the stator flux (V·s), predicted components in ($\alpha\beta$) axis of the rotor flux (V·s).

Also from $0.2s$ onwards with $\omega^* \neq 0$ and $T^* \neq 0$, using the three voltage vectors selected by the first control stage it is possible to control the torque. In fact, unlike what happened with the SMPC-FT2 strategy even in the istant in wich $|\boldsymbol{\lambda_s}^{k+2}| > |\boldsymbol{\lambda_s}^*|$ among the vectors selected by the first stage of control there is always a voltage vector that allows to obtain the desired torque adjustment. Consequently this vector will be selected from the second control stage and applied to the machine.

3.5 SMPC strategies that allow control of the induction motor

Given the high number of possible SMPC strategies, it was decided to summarize all the results obtained in this chapter in two tables. In particular, in Tab.3.2 are reported all the strategies, belonging to the SMPC-TF group, specifying whether they allow the induction motor control or not. In the same way, in Tab.3.3 all the strategies belonging to the SMPC-FT group are reported, specifying whether they allow the induction motor control or not.

Table 3.2: Strategies belonging to group SMPC-TF that allow to control the induction motor, with in detail the number of vectors used for the evaluation of the cost functions defined in the two stages.

STRATEGY	Number of voltage vector used for the evaluation of g_T	Number of voltage vector used for the evaluation of g_λ	Allow to control the induction motor
$SMPC\text{-}TF2$	7	2	Yes
$SMPC\text{-}TF3$	7	3	Yes
$SMPC\text{-}TF4$	7	4	No
$SMPC\text{-}TF5$	7	5	No
$SMPC\text{-}TF6$	7	6	No

Table 3.3: Strategies belonging to group SMPC-FT that allow to control the induction motor, with in detail the number of vectors used for the evaluation of the cost functions defined in the two stages.

STRATEGY	Number of voltage vector used for the evaluation of g_λ	Number of voltage vector used for the evaluation of g_T	Allow to control the induction motor
$SMPC\text{-}FT2$	7	2	No
$SMPC\text{-}FT3$	7	3	Yes
$SMPC\text{-}FT4$	7	4	Yes
$SMPC\text{-}FT5$	7	5	Yes
$SMPC\text{-}FT6$	7	6	Yes (high ripple)

4
Modulated Sequential Model Predictive control

The Sequential Model Predictive control (SMPC) stratgies are a new innovation in the field of high performance electric drives. With these strategies all the problems of definition of the weighting factors, typical Finite Control Set-Model Predictive Control (FCS-MPC) of torque and flux, can be considered solved. Since these strategies realize the minimization of the cost functions associated to the flux g_λ and torque g_T in two different control stages. In particular, at each control stage the number of usable voltage vectors is reduced, and finally the optimal voltage vector selected from the second control stage is applaied through the inverter. In Chapter 3 all the possible SMPC strategies that use two control stages to control stator flux and torque separately are presented, identifying which of them allow to control the induction machine (IM) when a 2 Level-Voltage Supplay Inverter (2L-VSI) is used to power it.

Like the FCS-MPC of torque and flux all the SMPC strategies present the disadvantage of the variable frequency switching (f_{sw}). In particular, f_{sw} is practically random and depends only on the operating conditions of the electric drive. In fact, once the sampling time has been set, the only limit for f_{sw} that cannot be exceeded is $1/(2 \cdot T_s)$, therefore any f_{sw} between zero and $1/(2 \cdot T_s)$ is possible. This causes a high harmonic spectrum of the currents and voltages at the inverter output. Such a wide harmonic spectrum of currents and voltage increases the losses in the iron and copper of the induction motor (IM) (and any other machine connected to the inverter), and also degrades the performance in terms of torque/speed ripple of the electric drive. Furthermore, the vector selected as a global optimum and used to supply the IM, is applied for the entire control period causing a high ripple on the controlled variables. In fact, in many cases there is no need to apply the vector for the entire control period so that the error of the controlled variable is canceled.

The main contribution of this thesis is the resolution of the problems just illustrated, implementing the modulation to the 2 Level Voltage Supply Inverter (2L-VSI). In particular, two modulation techniques have been studied and applied to the SMPC-FT3 strategy, that we will call two-vector modulation and three-vector modulation. With the two-vector modulation, after the two control stages, the duty-cycles of the optimal voltage vector and the zero voltage vector are calculated on the basis of the predicted torque

slope. The predicted torque slope is computed considering the case in which they were used for the all control period T_s to supplay the IM. With the three-vector modulation, after the two control stages, the duty-cycle of the optimum, of the second optimum and of the zero voltage vector are calculated on the basis the weighted average of the benefits, brought in terms of reduction of the torque error, if each of them is used to supplay the IM for all the control period.

The reasons why these modulation techniques have been introduced on SMPC-FT3 strategy are different. The first of all is the expected improvement of the performance in terms of current/torque ripple, using to supply the IM the voltage vectors selected from the second control stage based on the minimization of g_T and not of g_λ. In other words, the goal was, to supply the IM with the optimal voltage vectors for the minimization of the torque error and not with the optimal voltage vectors for the minimization of the flux error. This reason, is also what led to the study of the new SMPC-FT control strategies in which the evaluation of the cost functions is carried out in an inverse way compared to [18]. In any case, some equivalent modulation techniques to those used for the SMPC-FT3 strategy were tested also for the strategies belonging to the SMPC-TF group, but without success. The main problem, is that the voltage vectors selected and modulated in this case are positioned near the stator flux, while in the SMPC-FT case near the back electromotive force. Consequently, modulating voltage vectors positioned near the back electromotive force prevents the currents from having important variations, which instead does not happen by modulating voltage vectors near the stator flux. Finally, among all the possible SMPC-FT strategies that can be used the SMPC-FT3 was chosen, because without modulation an increase in the torque ripple was noticed, due to the increased number of voltage vectors available for the minimization of g_T which generally cause an increase in stator flux ripple.

In this Chapter, we will present the results obtained from the simulations by implementing the two modulation techniques illustrated and the mathematical formulation used for calculating the duty-cycles. In particular, the benefits introduced by the two modulation techniques will be observed, compared to the SMPC-FT3 case without modulation. The figures of merit analyzed will be the THD% of the currents and the amplitude of the torque ripple. With the aim of highlighting the excellent dynamic performance of this new control strategy, with and without modulation, the results obtained by carrying out a torque control of the machine without any speed loop are reported.

4.1 Torque control with the SMPC-FT3 strategy without modulation

The SMPC-FT3 strategy, start from the evaluation of g_λ by making the difference between the refence stator flux $|\boldsymbol{\lambda_s}^*|$ and the predicted stator flux

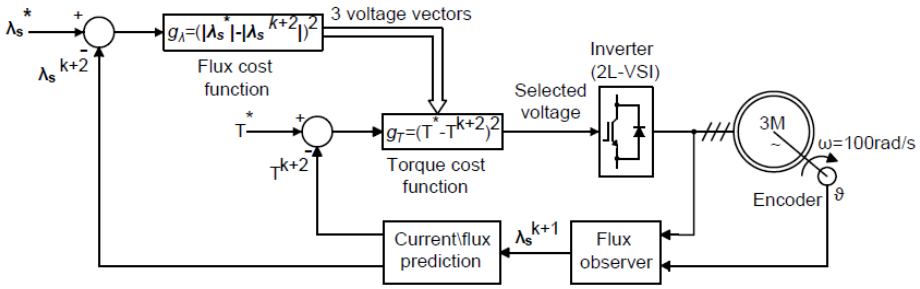

Figure 4.1: Block diagram, of torque control, based on the SMPC-FT3 strategy without modulator.

$|\boldsymbol{\lambda_s}^{k+2}|$ for all seven voltage vectors available from 2L-VSI. Then the three voltage vectors that generate the smallest value of g_λ and that at same time have the smallest subscription are used to calculate T^{k+2}. Finally, known T^* it is possible to proceed with the evaluation of the g_T for all the three available voltage vectors. Between the three available voltage vectors, the voltage vector that minimizes g_T and that at same time have the smallest subscription is selected as global optimal and applied through the inverter. Fig.4.1 shows the block diagram in case the SMPC-FT3 strategy is used directly to control torque.

The main parameters of the simulated machine can be found in Tab.2.1 and Tab.2.2, in addition the upper limit for switching frequency was set at 16 kHz. During the whole simulation the speed of the machine has been set equal to 100 rad/s. To verify the dynamic performance of the strategy, the dynamic response to the step change in torque was observed. In particular, from 0 s to 0.5 s the torque reference was set to 50 Nm while at 0.5 s it was set at -50 Nm, imposing a step change.

From Fig.4.2 it is possible to observe the fast dynamic response of the mechanical torque (T), which corresponds to a reversal of mechanical power from 5 kW to -5 kW in just 1.54 ms. Moreover, it is possible to note that the peak-to-peak ripple amplitude of the T is equal to 5 Nm, i.e. equal to 10% of the torque supplied by the machine. At the same way, the peak-to-peak ripple amplitude of the predicted torque (T^{k+2}) is similar to that of T. This allows us to state that all current and flux prediction are almost correct. One of the causes of this ripple is also due to the use of voltage vectors not modulated in amplitude for the power supply of the IM.

Fig.4.2 also shows the reference, the predicted amplitude and the component in the fixed reference frame ($\alpha\beta$) of the stator flux, it is interesting to observe the decoupling between the amplitude of the predicted stator flux ($|\boldsymbol{\lambda_s}^{k+2}|$) and the torque, despite the sequential evaluation of the cost functions related to the stator flux g_λ and torque g_T.

Finally, Fig.4.2 shows the stator currents in the reference ($\alpha\beta$), and the value of the $THD\%$ calculated, in steady state, during the generator

operation considering all current harmonics.

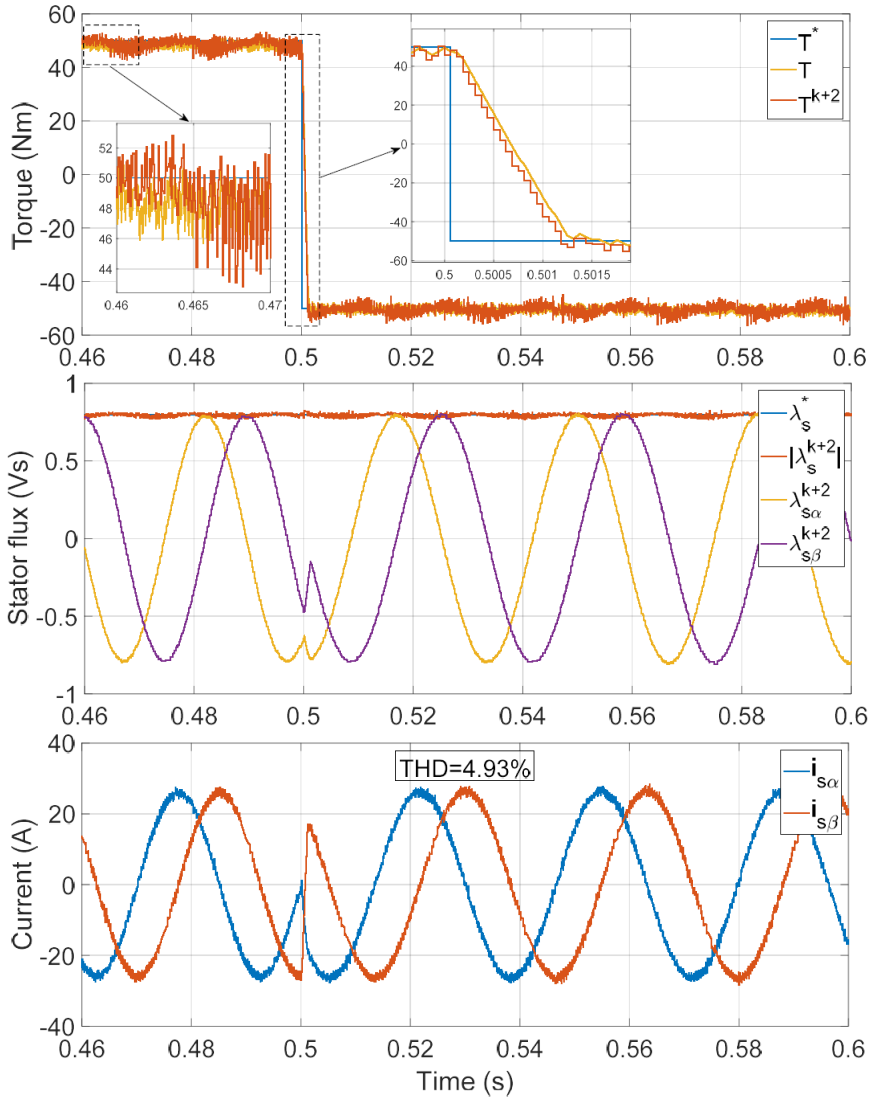

Figure 4.2: Torque step response from + 50Nm to -50Nm using the SMPC-FT3 strategy without modulation. From top to bottom: reference, deliver motor and predicted torque (N·m); magnitude reference, magnitude predicted and predicted components in ($\alpha\beta$) axis of the stator flux (V·s), feedback component in ($\alpha\beta$) axis of the current (A).

4.2 Torque control with the SMPC-FT3 strategy with modulation

As noted above, two modulation techniques have been studied and analyzed for the SMPC-FT3 strategy. As in the case without modulation, for both the modulation techniques, the torque control was analyzed.

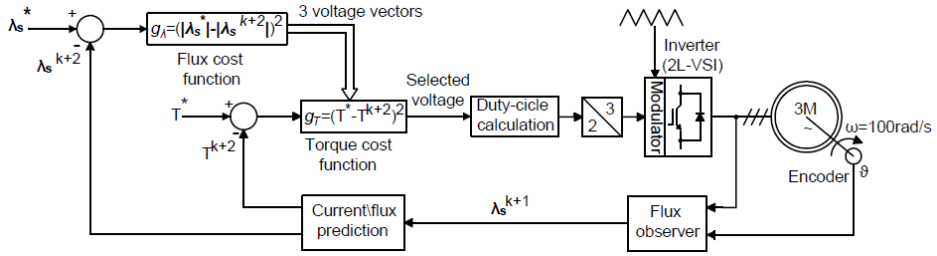

Figure 4.3: Block diagram of torque control based on the SMPC-FT3 strategy with modulator.

Furthermore, for both modulation techniques the procedure used in the simulations is identical to the case without modulation, i.e. for the whole simulation the rotation speed is set at 100 rad/s, and at 0.5 s the torque reference is changed from +50 Nm to -50 Nm. The main parameters of the simulated machine are shown in Tab.2.1 and Tab.2.2, during these simulations the switching frequency was set at 16 kHz. In Fig.4.3 is shown the block diagram which can be considered valid for the two-vector modulation and for the three-vector modulation.

4.2.1 Two vector modulation

With the two-vector modulation, after the two control stages, the duty-cycles of the optimal voltage vector and the zero voltage vector are calculated on the basis of the predicted torque slope. The predicted torque slope, is computed considering the case in which they were used for the all control period (T_s) to supply the IM. For the two vector modulation, it is necessary to distinguish the case in which the selected voltage vector as optimum is a non-zero voltage vector or is the zero voltage vector. So, let's call the generic non-zero voltage vector selected as optimal $\boldsymbol{v_{n0}}$, where the subscript "$n0$" stands for non-zero, while $\boldsymbol{v_0}$ the voltage vector zero. In fact, in the case the optimum is a generic voltage vector $\boldsymbol{v_{n0}}$, before being used to supplay the IM, it is modulated in amplitude; while in the case in witch the optimum is the voltage vector $\boldsymbol{v_0}$ it is directly used to supply the machine.

For the modulation of $\boldsymbol{v_{n0}}$ a coefficient called duty-ratio (d_r) is used. The d_r is calculated so as to be able to have, within of T_s, the predicted torque (T^{k+2}) equal to the reference torque (T^*). For the calculation of d_r the derivative of the predicted torque, in the case in which to supply the IM the voltage vector $\boldsymbol{v_{n0}}$ or $\boldsymbol{v_0}$ were used . We will call the two different torque derivatives $s_{\boldsymbol{v_{n0}}}$ and $s_{\boldsymbol{v_0}}$; more generally all the quantities calculated using the generic voltage vector $\boldsymbol{v_{n0}}$ or $\boldsymbol{v_0}$ will have the subscript respectively $\boldsymbol{v_{n0}}$ and $\boldsymbol{v_0}$.

The derivatives of the predicted torque calculated for the voltage vector $\boldsymbol{v_{n0}}$ and $\boldsymbol{v_0}$, shown respectively in (4.1) and (4.2), can be obtained by

deriving the equation of the torque (2.46).

$$s_{\boldsymbol{v_{n0}}} = \frac{dT^{k+2}_{\boldsymbol{v_{n0}}}}{dt} = \frac{3}{2}p\left(\frac{d\boldsymbol{\lambda}^{k+2}_{\boldsymbol{s,v_{n0}}}}{dt} \wedge \boldsymbol{i}^{k+2}_{\boldsymbol{s,v_{n0}}} - \frac{d\boldsymbol{i}^{k+2}_{\boldsymbol{s,v_{n0}}}}{dt} \wedge \boldsymbol{\lambda}^{k+2}_{\boldsymbol{s,v_{n0}}}\right) \tag{4.1}$$

$$s_{\boldsymbol{v_0}} = \frac{dT^{k+2}_{\boldsymbol{v_0}}}{dt} = \frac{3}{2}p\left(\frac{d\boldsymbol{\lambda}^{k+2}_{\boldsymbol{s,v_0}}}{dt} \wedge \boldsymbol{i}^{k+2}_{\boldsymbol{s,v_0}} - \frac{d\boldsymbol{i}^{k+2}_{\boldsymbol{s,v_0}}}{dt} \wedge \boldsymbol{\lambda}^{k+2}_{\boldsymbol{s,v_0}}\right) \tag{4.2}$$

The quantities $\boldsymbol{i}^{k+2}_{\boldsymbol{s,v_{n0}}}$ and $\boldsymbol{\lambda}^{k+2}_{\boldsymbol{s,v_{n0}}}$ can be calculated using the equations (3.12) and (3.13). In particular, their expressions in a vector form are reported in equations (4.3) and (4.4).

$$\boldsymbol{i}^{k+2}_{\boldsymbol{s,v_{n0}}} = \boldsymbol{i}^{k+1}_{\boldsymbol{s}} + \frac{T_s}{\sigma L_s}\left(\boldsymbol{v}^{k+1}_{\boldsymbol{n0}} - \left(R_s + R_r\frac{L_s}{L_r} - j\omega\sigma L_s\right)\boldsymbol{i}^{k+1}_{\boldsymbol{s}} + \left(\frac{1}{\tau_r} - j\omega\right)\boldsymbol{\lambda}^{k+1}_{\boldsymbol{s}}\right) \tag{4.3}$$

$$\boldsymbol{\lambda}^{k+2}_{\boldsymbol{s,v_{n0}}} = \boldsymbol{\lambda}^{k+1}_{\boldsymbol{s}} + T_s\boldsymbol{v}^{k+1}_{\boldsymbol{n0}} - T_sR_s\boldsymbol{i}^{k+1}_{\boldsymbol{s}} \tag{4.4}$$

From the equations (4.3) and (4.4) the equation that allow to calculate $d\boldsymbol{i}^{k+2}_{\boldsymbol{s,v_{n0}}}/dt$ and $d\boldsymbol{\lambda}^{k+2}_{\boldsymbol{s,v_{n0}}}/dt$ can easily be obtained, they are shown in the equations (4.5) and (4.6).

$$\frac{d\boldsymbol{i}^{k+2}_{\boldsymbol{s,v_{n0}}}}{dt} = \frac{1}{\sigma L_s}\left(\boldsymbol{v}^{k+1}_{\boldsymbol{n0}} - \left(R_s + R_r\frac{L_s}{L_r} - j\omega\sigma L_s\right)\boldsymbol{i}^{k+1}_{\boldsymbol{s}} + \left(\frac{1}{\tau_r} - j\omega\right)\boldsymbol{\lambda}^{k+1}_{\boldsymbol{s}}\right) \tag{4.5}$$

$$\frac{d\boldsymbol{\lambda}^{k+2}_{\boldsymbol{s,v_{n0}}}}{dt} = \boldsymbol{v}^{k+1}_{\boldsymbol{n0}} - R_s\boldsymbol{i}^{k+1}_{\boldsymbol{s}} \tag{4.6}$$

The relationships necessary for the calculation of $d\boldsymbol{\lambda}^{k+2}_{\boldsymbol{s,v_0}}/dt$, $\boldsymbol{i}^{k+2}_{\boldsymbol{s,v_0}}$, $\boldsymbol{i}^{k+2}_{\boldsymbol{s,v_0}}/dt$ and $\boldsymbol{\lambda}^{k+2}_{\boldsymbol{s,v_0}}$ are completely analogous to those just illustrated for the voltage vector $\boldsymbol{v_{n0}}$. They can be obtained by setting $\boldsymbol{v_{n0}} = 0$ in the equations (4.3), (4.4), (4.5) and (4.6).

Calculate the derivatives of the torque, d_r is easily calculated. To clarify the operating principle refer to Fig.4.4, where a generic operating interval is considered and in which the predicted torque at the instant $k+1$ i.e. T^{k+1} is less than the reference one (T^*). We assume that the generic voltage vector $\boldsymbol{v_{n0}}$ selected at the instant $k+1$ is able to increase the torque delivered by the machine while $\boldsymbol{v_0}$ to reduce it. Therefore, considering that the control objective is to be able to obtain at the end of the control period (i.e. at the instant $k+2$) a zero torque error, is intuitive that to do this, the following equation must be respected:

$$E^{k+2}_T = |E^{k+1}_T + s_{\boldsymbol{v_{n0}}}d_rT_s + s_{\boldsymbol{v_0}}(1-d_r)T_s| = 0 \tag{4.7}$$

where E^{k+1}_T and E^{k+2}_T are respectively the torque errors at time $k+1$ and at that $k+2$, calculable using equations (4.8) and (4.9).

$$E_T^{k+1} = (T^{k+1} - T^*) \tag{4.8}$$

$$E_T^{k+2} = (T^{k+2} - T^*) \tag{4.9}$$

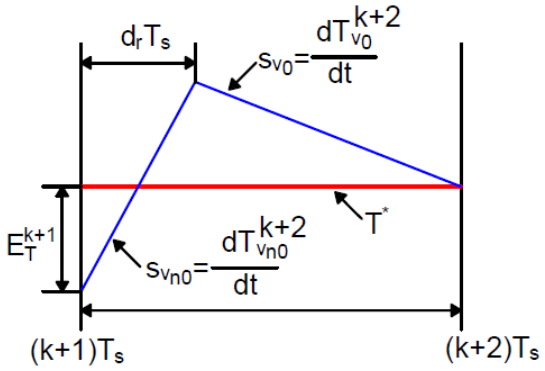

Figure 4.4: Generic operating interval, in which the torque error at the instant $k+1$ is equal to E_T^{k+1} while at the instant $k+2$ is zero. The blue line identifies the derivatives of the predicted torque calculated using the generic vector $\boldsymbol{v_{n0}}$ and $\boldsymbol{v_0}$ while the red line identifies the reference torque, finally $d_r T_s$ indicates the time of use of the vector $\boldsymbol{v_{n0}}$ to supply the machine.

Similar considerations can be made in the case where at the instant $k+1$ the predicted torque (T^{k+1}) is greater than the reference one (T^*). It remains to be observed that the use of the voltage vector $\boldsymbol{v_0}$ for the all control period, when it is selected as the optimal voltage vector does not allow to satisfy the equation (4.7). This is a simplification made in the implementation phase, because otherwise it would have been necessary to calculate the $\boldsymbol{s_{v_{n0}}}$ for all six voltage vectors different from zero, and identify which of the six if modulated in amplitude would have allowed us to obtain at the end of the control step $E_T^{k+2} = 0$. In this way, we have tried not to over-complicate the implementation of the control and in any case, despite this simplifying choice, clear improvements were obtained with respect to the SMPC-FT3 case without modulation.

By performing the steps, using the equation (4.7), it is possible to obtain the equation (4.10) that allows to calculate the d_r.

$$d_r = -\frac{s_{\boldsymbol{v_0}} T_s + E_T^{k+1}}{T_s(s_{\boldsymbol{v_{n0}}} - s_{\boldsymbol{v_0}})} \tag{4.10}$$

Calculated d_r, and limited within [0,1] it is possible to define the stator voltage $\boldsymbol{v_s}$ in the fixed stator reference frame ($\alpha\beta$) using the equation (4.11). Finally using the transformation of the controllers $\boldsymbol{B}$ it is possible to define the three phase voltages.

$$\boldsymbol{v_s} = \boldsymbol{v_{n0}} d_r \tag{4.11}$$

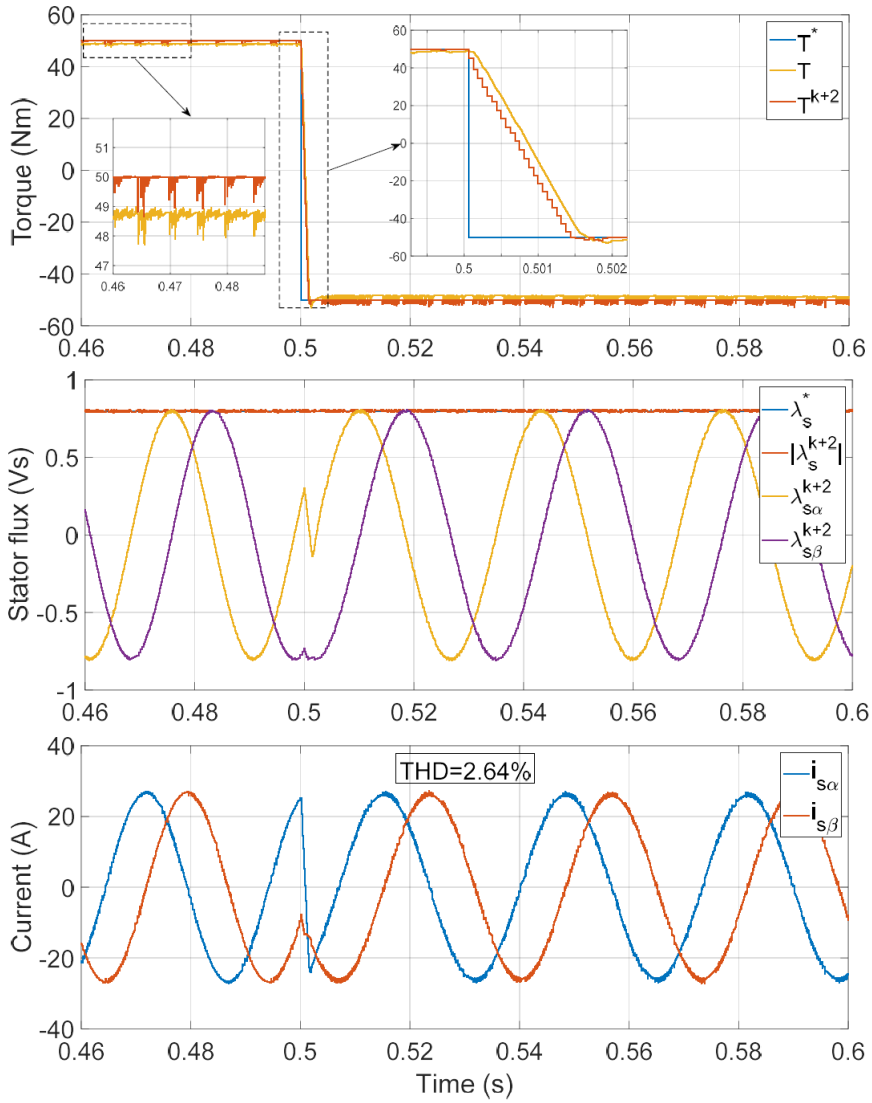

Figure 4.5: Torque step response from +50Nm to -50Nm using the SMPC-FT3 strategy with two-vector modulation. From top to bottom: reference, deliver motor and predicted torque (N·m); magnitude reference, magnitude predicted and predicted components in ($\alpha\beta$) axis of the stator flux (V·s), feedback component in ($\alpha\beta$) axis of the current (A).

Fig.4.5 shows the results obtained using this new modulation technique. In particular it is interesting to observe the important reduction in torque ripple of T and of T^{k+2}. For T and T^{k+2} the amplitude of the peak-to-peak ripple does not exceed 1.5 Nm which is equivalent the 3% of the torque supplied by the IM. In other words, this means that by using the two vector modulation a torque ripple reduction of 70% is obtained compared to the case without modulation. Moreover it is possible to observe that the time

taken to realize the torque inversion remains approximately analogous to the case without modulation. It is also important to observe the presence of a stationary error between the predicted torque T^{k+2} and the torque actually delivered by the machine T, which in the case without modulation could not be appreciated due to the high torque ripple. This stationary error is caused by considering the phenomena of iron losses and magnetic saturation in the model of the simulated machine, but not in the equations used for the implementation of SMPC strategies. In fact, in order to predict currents and flux, the non-saturated magnetization inductance value is used and the losses in the iron are not considered.

Moreover from Fig.4.5, it is possible to observe how even introducing voltage vector modulation and carrying out a sequential evaluation of the cost functions $g\lambda$ and g_T, it is possible to obtain the decoupling between stator flux and torque.

Finally, it is important to note that thanks to the use of this modulation technique it is also possible to obtain a reduction of the $THD\%$ of currents equal to 46.5% compared to the case without modulation, $THD\%$ calculated considering all the harmonics present.

4.2.2 Three vector modulation

With the three-vector modulation, after two control stages, the duty-cycle of the optimum, of the second optimum and of the zero voltage vector are calculated. These duty-cycle, are calculated on the basis of the weighted average of the benefits, brought in terms of reduction of the torque error, if each of them is used to supplay the IM for all the control period.

We will call the optimal, the second optimal and the zero voltage vectors respectively $\boldsymbol{v_{opt1}}$, $\boldsymbol{v_{opt2}}$ and $\boldsymbol{v_0}$; while the benefits associated at each of them $b_{\boldsymbol{v_0}}$, $b_{\boldsymbol{v_{opt1}}}$ and $b_{\boldsymbol{v_{opt2}}}$. The benefits $b_{\boldsymbol{v_0}}$, $b_{\boldsymbol{v_{opt1}}}$ and $b_{\boldsymbol{v_{opt2}}}$ are calculated using the following equation:

$$b_{\boldsymbol{v_0}} = \frac{1}{|T^* - T^{k+2}_{\boldsymbol{v_0}}|} \tag{4.12}$$

$$b_{\boldsymbol{v_{opt1}}} = \frac{1}{|T^* - T^{k+2}_{\boldsymbol{v_{opt1}}}|} \tag{4.13}$$

$$b_{\boldsymbol{v_{opt2}}} = \frac{1}{|T^* - T^{k+2}_{\boldsymbol{v_{opt2}}}|} \tag{4.14}$$

where T^* is the reference torque, while $T^{k+2}_{\boldsymbol{v_0}}$, $T^{k+2}_{\boldsymbol{v_{opt1}}}$ and $T^{k+2}_{\boldsymbol{v_{opt2}}}$ are the predicted torque, at instant $k+2$, computed using the voltage vectors $\boldsymbol{v_0}$, $\boldsymbol{v_{opt1}}$ and $\boldsymbol{v_{opt2}}$ as indicated by their subscripts. All the three predicted torque can be calculated using the equations (3.12), (3.13) and (3.14) presented in Chapter 3.

Known $b_{\boldsymbol{v_0}}$, $b_{\boldsymbol{v_{opt1}}}$ and $b_{\boldsymbol{v_{opt2}}}$, making their weighted average, it is possible to define the duty-cycle to be associated at each of the three voltage vectors. So, we will call the three duty-cycles $d_{\boldsymbol{v_0}}$, $d_{\boldsymbol{v_{opt1}}}$ and $d_{\boldsymbol{v_{opt2}}}$, where subscripts allow us to identify at which voltage vector, each of them must be applied.

However, to correctly calculate the weighted average of the benefits and therefore the duty-cycle it is necessary to distinguish three cases, so as not to overestimate the benefits brought by the single voltage vectors. The three cases that must be distinct are:

- $\boldsymbol{v_{opt1}} \neq \boldsymbol{v_0}$, $\boldsymbol{v_{opt2}} \neq \boldsymbol{v_0}$;
- $\boldsymbol{v_{opt1}} = \boldsymbol{v_0}$, $\boldsymbol{v_{opt2}} \neq \boldsymbol{v_0}$;
- $\boldsymbol{v_{opt1}} \neq \boldsymbol{v_0}$, $\boldsymbol{v_{opt2}} = \boldsymbol{v_0}$;

In fact, for each of the three cases just mentioned, the duty-cycle calculation changes as shown below:

$$\text{if } \boldsymbol{v_{opt1}} \neq \boldsymbol{v_0} \text{ and } \boldsymbol{v_{opt2}} \neq \boldsymbol{v_0} \Rightarrow \begin{cases} d_{\boldsymbol{v_0}} = \frac{b_{\boldsymbol{v_0}}}{b_{\boldsymbol{v_0}}+b_{\boldsymbol{v_{opt1}}}+b_{\boldsymbol{v_{opt2}}}}; \\ d_{\boldsymbol{v_{opt1}}} = \frac{b_{\boldsymbol{v_{opt1}}}}{b_{\boldsymbol{v_0}}+b_{\boldsymbol{v_{opt1}}}+b_{\boldsymbol{v_{opt2}}}}; \\ d_{\boldsymbol{v_{opt2}}} = \frac{b_{\boldsymbol{v_{opt2}}}}{b_{\boldsymbol{v_0}}+b_{\boldsymbol{v_{opt1}}}+b_{\boldsymbol{v_{opt2}}}}; \end{cases} \tag{4.15}$$

$$\text{if } \boldsymbol{v_{opt1}} = \boldsymbol{v_0} \text{ and } \boldsymbol{v_{opt2}} \neq \boldsymbol{v_0} \Rightarrow \begin{cases} d_{\boldsymbol{v_0}} = \frac{b_{\boldsymbol{v_0}}}{b_{\boldsymbol{v_0}}+b_{\boldsymbol{v_{opt2}}}}; \\ d_{\boldsymbol{v_{opt1}}} = 0; \\ d_{\boldsymbol{v_{opt2}}} = \frac{b_{\boldsymbol{v_{opt2}}}}{b_{\boldsymbol{v_0}}+b_{\boldsymbol{v_{opt2}}}}; \end{cases} \tag{4.16}$$

$$\text{if } \boldsymbol{v_{opt1}} \neq \boldsymbol{v_0} \text{ and } \boldsymbol{v_{opt2}} = \boldsymbol{v_0} \Rightarrow \begin{cases} d_{\boldsymbol{v_0}} = \frac{b_{\boldsymbol{v_0}}}{b_{\boldsymbol{v_0}}+b_{\boldsymbol{v_{opt1}}}}; \\ d_{\boldsymbol{v_{opt1}}} = \frac{b_{\boldsymbol{v_{opt1}}}}{b_{\boldsymbol{v_0}}+b_{\boldsymbol{v_{opt1}}}}; \\ d_{\boldsymbol{v_{opt2}}} = 0. \end{cases} \tag{4.17}$$

Defined the duty-cycles in the three possible cases, it is possible to define the voltage in the reference frame ($\alpha\beta$) using equation (4.18), and finally define the three phase voltages using the transformation of the controllers $\boldsymbol{B}$.

$$\boldsymbol{v_s} = \boldsymbol{v_0} d_{\boldsymbol{v_0}} + \boldsymbol{v_{opt1}} d_{\boldsymbol{v_{opt1}}} + \boldsymbol{v_{opt2}} d_{\boldsymbol{v_{opt2}}} \tag{4.18}$$

Fig.4.6 shows the results obtained using three vector modulation technique. It is interesting to observe how with this technique a further reduction in a torque ripple is obtained compared to the two-vector modulation technique, in fact the peak-to-peak ripple amplitude of the torque deliver by the IM does not exceed 1 Nm. This amplitude torque ripple is equal to 2% of the torque delivered by the machine, and furthermore this means an improvement in torque ripple amplitude compared to the case without modulation

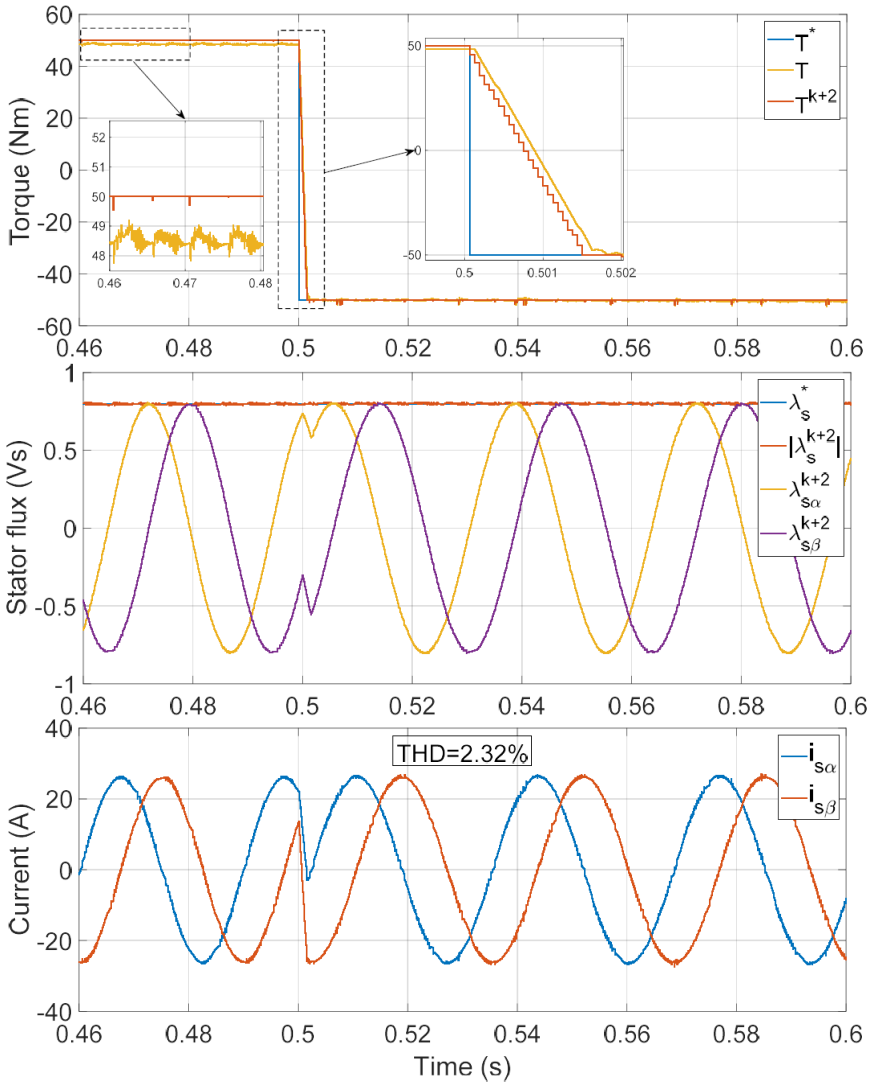

Figure 4.6: Torque step response from + 50Nm to -50Nm using the SMPC-FT3 strategy with three vector modulation. From top to bottom: reference, deliver motor and predicted torque (N·m); magnitude reference, magnitude predicted and predicted components in ($\alpha\beta$) axis of the stator flux (V·s), feedback component in ($\alpha\beta$) axis of the current (A).

equal to 80%. Also in this case, it is possible to observe the presence of a stationary error between the predicted torque and the torque delivered by the machine, the reasons for which this error is present, are the same as in the previous case. From Fig.4.6, it is possible to observe how also in this case the decoupling between the flux and the torque is guaranteed despite the sequential evaluation of the stator flux and torque error.

Finally, with the three vector modulation we can observe a further im-

provement of the $THD\%$, in particular an improvement of the $THD\%$ is obtained with respect to the case without modulation equal to 53%; THD calculated considering all the currents harmonics.

5
Experimental analysis

To validate the results obtained from the simulations, using the Matlab/Simulink software, experimental tests were conducted on the new control strategies based on the Sequential Model Predictive Control (SMPC). The experimental tests were conducted in the Power Electronics, Machines and Control (PEMC) laboratory of the University of Nottingham. In this Chapter the most significant results of the experimental tests conducted are shown. In particular, the results obtained from the tests conducted using the SMPC-FT3 strategy without modulation and the SMPC-FT3 strategy with the three vector modulation technique are presented.

In the first section of this chapter the experimental setup used during the experimental tests is shown, in addition the test bench used is also shown and briefly described. In the second section the results obtained from the experimental tests are illustrated. In particular, as already done in the simulations shown in Chapter 4, the experimental tests have been conducted realizing the IM torque control at constant speed.

5.1 Test bench

To verify and validate experimentally the torque control of the three phase induction motor (IM), using the different control strategies presented in the previous chapters, the IM was coupled with a permanent magnet synchronous machine (PMSM), the experimental setup is shown in the photo of Fig.5.1.

The PMSM was used to control the rotation speed during the test phases of the IM torque control, based on the SMPC-FT3 without modulation and SMPC-FT3 with modulation strategies. To control the speed of the PMSM an industrial driver was used, while for the IM torque control the algorithms were loaded on a custom DSP/FPGA board. In particular, the custom DSP/FPGA processed and sent duty-cycles to the industrial three-phase inverter used to supply the IM. The control algorithms used are based on the theory presented in Chapter 3 and in Chapter 4. In Fig.5.2 a schematic version of the test bench used is presented.

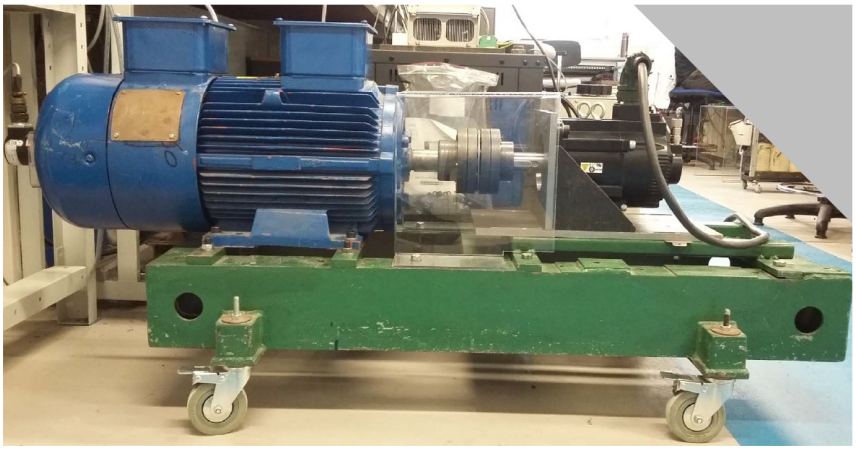

Figure 5.1: Experimental setup: on the left the IM, on the right the PMSM.

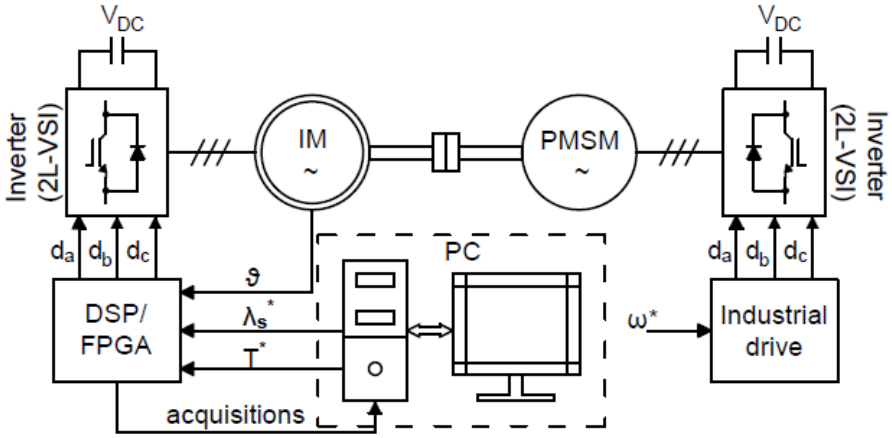

Figure 5.2: Schematic representation of the test bench.

5.2 Experimental results

The main parameters and the nameplate of the IM, used to test the two different strategies, are reported respectively in Table 2.1 and Table 2.2, while in Table 5.1 the main control parameters used in the experimental tests are shown.

After the first phase of setting up the test bench, during which the measurements of all the signals necessary for the implementation of control strategies were verified, the experimental tests were carried out. During this phase the main problems encountered occurred on the encoder reset command signal. In fact, during some tests a sudden and incorrect reset of the encoder was observed which caused, the loss of IM torque control. These problems, due to the presence of high electromagnetic disturbances present

during operation, are solved by carefully arranging of the electrical power cables and of the electrical signal cables and introducing some blocking coils on the electric cables used to read the signals of the encoder.

Table 5.1: Main parameters used during the experimental tests.

Parametrers	Value
Incremental encoder	25000 *pulse per revolution*
DC-link voltage	520 V
Reference speed: ω^*	1000 rpm
Switching frequency	16 kHz
Sampling rate	32 kHz

5.2.1 Response to torque step using the SMPC-FT3 strategy without modulation

Fig.5.4 shows the results of the response to the step change of the torque reference from +50 Nm to -50 Nm using the SMPC-FT3 strategy, with the rotor speed of the IM held at 1000 rpm using the PMSM.

It is interesting to observe how in 1.2 ms a torque inversion can be obtained which corresponds to an inversion of mechanical power of approximately 10 kW. Moreover, it is possible to observe how the ripple on the predicted torque T^{k+2} at steady state, presents a peak-to-peak amplitude equal to 2.5 Nm. The T^{k+2} can be considered with a good approximation similar to the real torque delivered by the IM. In fact, at these speed values the flux estimation deriving from the flux observer is very accurate, the only possible errors are due to the magnetic saturation that was not considered in the implementation of the strategy.

In Fig.5.4 are shown the refence, the predicted and the component in a fixed frame ($\alpha\beta$) of the stator flux, and it is important to note that, actually even the experimental tests show the decoupling between the stator flux and torque in these working conditions, despite the evaluation of the cost functions attributed to torque and stator flux takes place in two separate stages. Decoupling, which can be observed during the torque transient and where it is observed that the predicted stator flux λ_s^{k+2} follows the stator flux reference λ_s^{k+2}

Finally, in Fig.5.4 the stator currents measured in alpha beta axes and the THD are shown. The THD is less than 5%, where 5% is generally taken as a reference value to assess whether there is presence or not of excessive harmonic distortion.

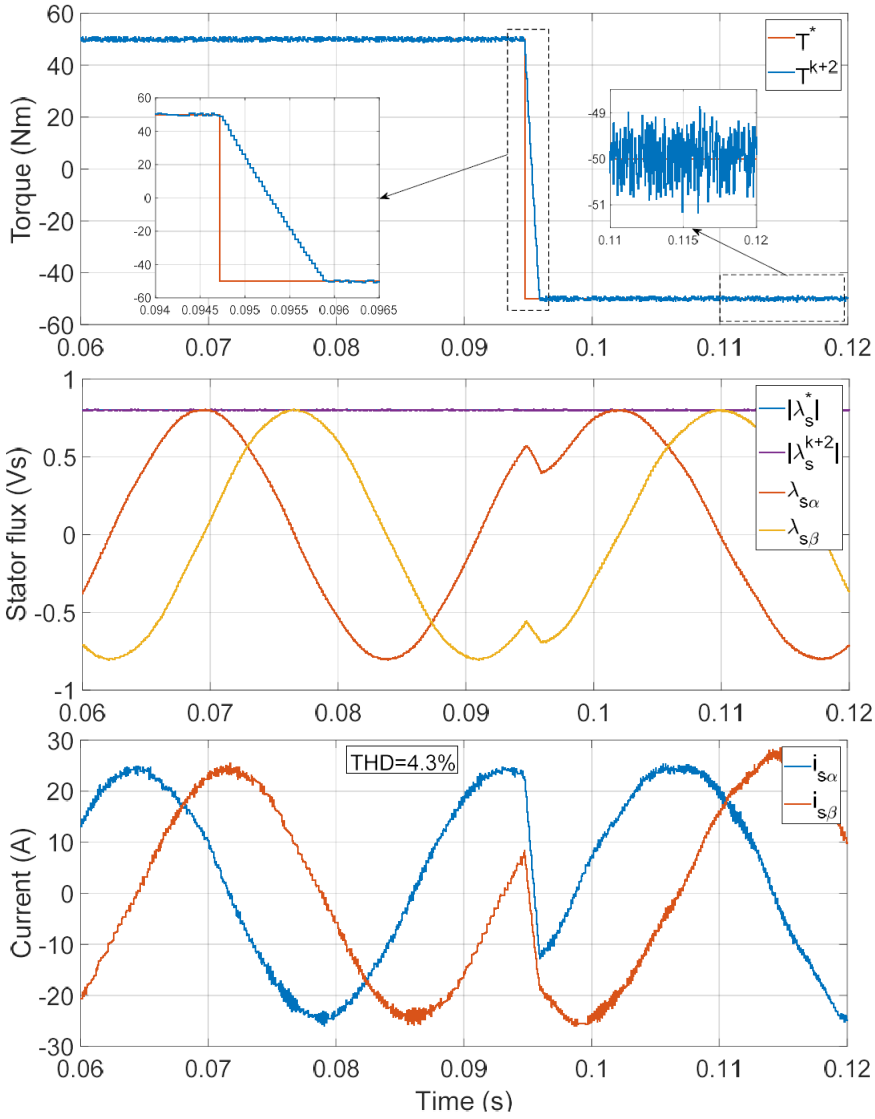

Figure 5.3: Experimental results for a torque step response from +50 Nm to -50 Nm using the SMPC-FT3 strategy without modulation. From top to bottom: reference and predicted torque(N·m); magnitude reference, magnitude predicted and predicted components in ($\alpha\beta$) axis of the stator flux (V·s), feedback component in ($\alpha\beta$) axis of the current (A).

5.2.2 Response to torque step using the SMPC-FT3 strategy with three-vector modulation

Fig.5.4 shows the results of the response to the step change of the torque reference from +50 Nm to -50 Nm using the SMPC-FT3 strategy with three vector modulation, when the rotor speed of the IM is held at 1000 rpm from the PMSM.

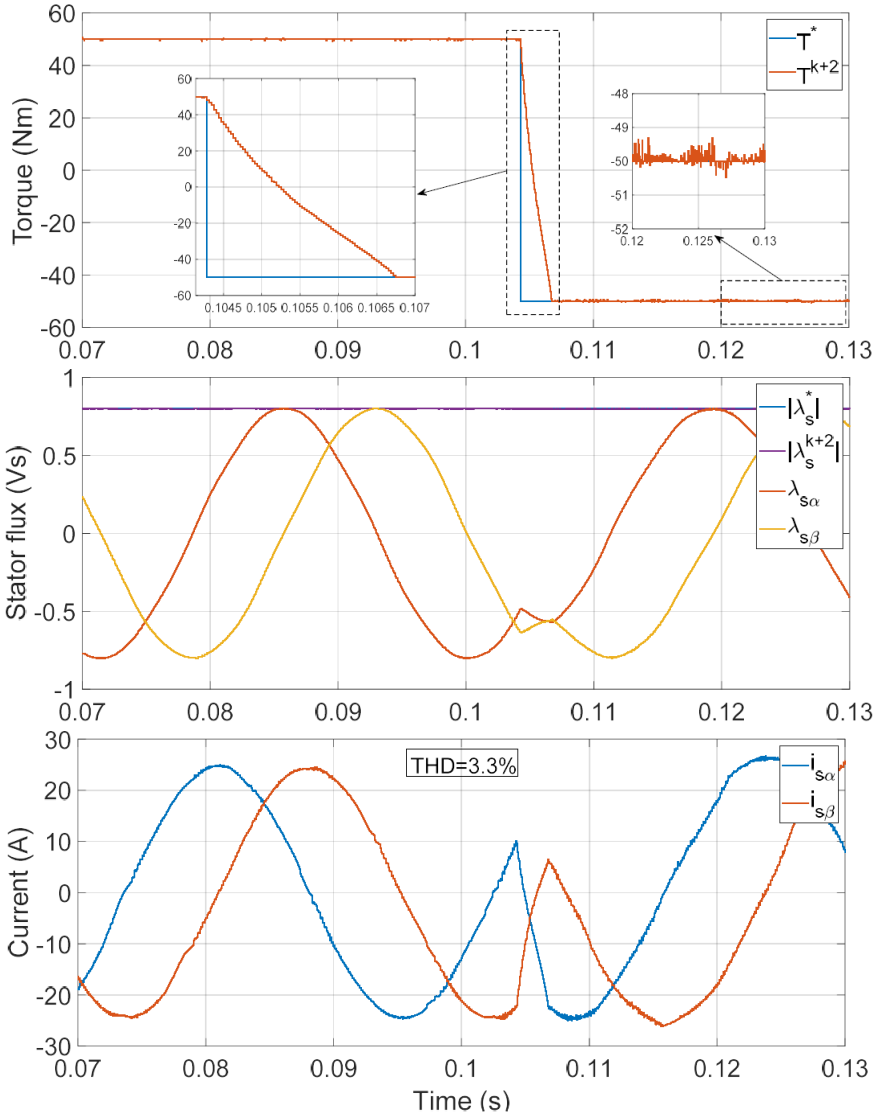

Figure 5.4: Experimental results for a torque step response from +50 Nm to -50 Nm using the SMPC-FT3 strategy with three vector modulation. From top to bottom: reference and predicted torque(N·m); magnitude reference, magnitude predicted and predicted components in ($\alpha\beta$) axis of the stator flux (V·s), feedback component in ($\alpha\beta$) axis of the current (A).

From the first experimental tests we observed an increase in the time required to perform the torque reversal, in fact with this strategy the time taken is equal to 2.3 ms. Increase of the necessary inversion time, which was also observed during the simulations of this modulation technique, but not so importantly. The main reason for this increase in time, necessary to effect the reversal of torque, could be due to the use of the second optimum

voltage vector for the definition of the supply voltage. In any case, this problem should be further investigated.

As actually expected, in Fig.5.4 it is also possible to observe the reduction of the torque ripple which has a peak-to-peak amplitude lower than 1 Nm at steady state, so it means that effectively a reduction equal to 60% of the ripple torque is obtained. Also in this, for the same reasons as the previous case, the predicted torque T^{k+2} can be considered a good estimate.

As shown in Fig.5.4, even using modulation, the decoupling between the stator flux and torque in these operating conditions is guaranteed, given that during the torque reversal the predicted flux follows the reference flux. Finally, from Fig.5.4 we can see how the $THD\%$ of the currents with the modulation is reduced, presenting an improvement equal to 23% compared to the case without modulation.

6
Conclusions and outlook

In this thesis various control strategies have been studied for a three-phase induction motor (IM) powered by 2-level-Voltage-Supply-Inverter (2L-VSI). In particular, all the strategies studied are based on the Sequential Model Predictive Control (SMPC).

The SMPC is a recent innovation in the high-performance control of electric drives that allows the elimination of the weighting factors. The elimination of weighting factors and associated tuning is one of the biggest advantages of this new strategies. The simulations, that I have carried, demonstrate the existence of six possible SMPC-type strategies that allow to control the IM. After a careful analysis of those various SMPC strategies, I have chosen the one that showed the lowest current and torque ripples and I have also implemented a modulator in order to make constant the switching frequency. In fact, like the conventional Finite-Control-Set-MPC, the SMPC also has an disadvantage of variable switching frequency. In particular, the modulation techniques introduced and applied to the chosen SMPC type strategy are two called two-vector modulation and three-vector modulation. The SMPC strategy chosen on which I have implemented modulation techniques is the SMPC-FT3 strategy.

Thanks to the implementation of the modulator it was possible to make constant the switching frequency and also reduce the torque and current ripple compared to the SMPC-FT3 case without modulator. After the simulation of all the possible SMPC strategies and the two modulation techniques, the SMPC-FT3 strategy without modulation and the SMPC-FT3 strategy with the three-vector modulation technique were validated experimentally.

In any case, there are many improvements that can be introduced to the SMPC strategies and modulation techniques. The first of all, could be the introduction of a look up table (LUT) with which to consider magnetic saturation, and therefore the variation of magnetization inductance as a function of current. With the introduction of this LUT the error at steady-state between the predicted torque and the torque actually delivered by the IM would be significantly reduced. In fact, this error is mainly caused by the incorrect prediction of the current since the magnetic saturation in the implemented strategies is not considered.

The second improvement that can be introduced is the implementation of the Space Vector Modulation, in such a way as to solve the problems

of over-switching present with the two modulation techniques studied and implemented, so as to be able to obtain a homogeneous exploitation of the power switches, and a better exploitation of the inverter.

Ringrazio la mia famiglia, sopratutto i miei genitori mia sorella e il segretario Eugenio, che mi hanno sempre sostenuto in tutto e per tutto, senza di loro tutto ciò non sarebbe stato possibile.

Ringrazio Davide, per l'aiuto datomi durante tutta la mia carriera universitaria e per i suoi continui e preziosi consigli di vita.

Ringrazio Cesare, che da sempre mi ha supportato e soprattutto sopportato anche come coinquilino qui a Torino.

Ringrazio Pasquale, per tutte le belle e intense giornate passate ad ogni mio ritorno a Ruvo che mi permettevano di rilassarmi e ricarmi. Se non ci sarai il giorno della discussione, è perchè purtroppo per te, è arrivato il momento di iniziare a lavorare.

Ringrazio Adriano e Laura, primi veri amici conosciuti qui a Torino ormai nel lontano 2011, da allora sempre presenti e disponibili.

Un grazie a Giulio, soprattutto per avermi reso più vivibili i primi anni qui a Torino, come dimenticare tutte le giornate passate in Via Bava!

Ringrazio Özge, per tutte le belle serate e le Domeniche passate all'insegna del buon cibo durante la mia tesi a Nottingham.

Infine, ringrazio i miei relatori, Prof. Radu Bojoi, Prof. Pericle Zanchetta, Dr.Shafiq Ahmed Odhano, Dr. Silvio Vaschetto, per tutti i consigli ricevuti e per l'opportunità datami di realizzare il presente lavoro di tesi presso la University of Nottingham.

Bibliography

[1] J. Rodriguez and P. Cortes, *Predictive control of power converters and electrical drives* (2012).

[2] E. F. Camacho and C. Bordons, *Model Predictive Control* (1999).

[3] C. E.García, D. M.Prett, and ManfredMorari, *Model predictive control: Theory and practice—A survey* (1989).

[4] J. Holtz and S. Stadtfeld, International Power Electronics Conference, IPEC, (1983).

[5] M. Norambuena, C. Garcia, and J. Rodriguez, in *2016 7th Power Electronics and Drive Systems Technologies Conference (PEDSTC)* (2016) pp. 636–640.

[6] S. A. Davari, D. A. Khaburi, P. Stolze, and R. Kennel, in *Proceedings of the 2011 14th European Conference on Power Electronics and Applications* (2011) pp. 1–10.

[7] J. Holtz, Proceedings of the IEEE **82**, 1194 (1994).

[8] I. Takahashi and Y. Ohmori, IEEE Transactions on Industry Applications **25**, 257 (1989).

[9] T. G. Habetler, F. Profumo, M. Pastorelli, and L. M. Tolbert, in *Conference Record of the 1991 IEEE Industry Applications Society Annual Meeting* (1991) pp. 428–436 vol.1.

[10] D. Stando and M. P. Kazmierkowski, in *2013 International Conference-Workshop Compatibility And Power Electronics* (2013) pp. 225–230.

[11] P. Cortes, J. Rodriguez, C. Silva, and A. Flores, Industrial Electronics, IEEE Transactions on **59**, 1323 (2012).

[12] A. Linder and R. Kennel, in *2005 IEEE 36th Power Electronics Specialists Conference* (2005) pp. 1793–1799.

[13] P. Cortes, M. P. Kazmierkowski, R. M. Kennel, D. E. Quevedo, and J. Rodriguez, IEEE Transactions on Industrial Electronics **55**, 4312 (2008).

[14] R. P. Aguilera, P. Lezana, and D. E. Quevedo, IEEE Transactions on Industrial Informatics **9**, 658 (2013).

[15] Z. Zhang, , , and R. Kennel, in *2017 IEEE Transportation Electrification Conference and Expo (ITEC)* (2017) pp. 84–89.

[16] P. Cortes, S. Kouro, B. La Rocca, R. Vargas, J. Rodriguez, J. I. Leon, S. Vazquez, and L. G. Franquelo, in *2009 IEEE International Conference on Industrial Technology* (2009) pp. 1–7.

[17] C. A. Rojas, J. Rodriguez, F. Villarroel, J. R. Espinoza, C. A. Silva, and M. Trincado, IEEE Transactions on Industrial Electronics **60**, 681 (2013).

[18] M. Norambuena, J. Rodriguez, Z. Zhang, F. Wang, C. Garcia, and R. Kennel, IEEE Transactions on Power Electronics **34**, 794 (2019).

[19] M.Lazzari, *Macchine elettriche 2*.

[20] A.Vagati, *Notes of the electric drives course, Polytechnic University of Turin*.

[21] A. K. A.E. Fitzgerald, C. Kingsley Jr., *Macchine elettriche* (2015).

[22] M.Lazzari, *Macchine elettriche 1*.

[23] A.Fratta, *Dispense del corso di Conversione Statica dell'Energia Elettrica* (1998).